LOCAL ELECTRON TRANSPORT OF ORGANIC SEMICONDUCTING MONOLAYERS

DANTI CHEN

SUBMITTED TO

PHYSICS DEPARTMENT, MOUNT HOLYOKE COLLEGE

KATHERINE AIDALA, MOUNT HOLYOKE COLLEGE

THESIS ADVISOR

MAY 2009

Acknowledgements

This thesis would not have been possible without the following people. I would like to give my sincere thanks to:

- My advisor Katherine Aidala for introducing me to this wonderful field of research and being the most supportive and inspirational figure along the way.
- Professor Janice Hudgings and Jessica Sidman for being willing to sit on my committee.
- Professor David Ginger and Professor Brad Orr for research related tips and suggestions.
- Physics department for being extremely supportive and the rest of physics majors/minors for being my family at Mount Holyoke College.

- My lab mates, especially Tolu Ogunbekun with whom I shared a project two years ago, for sharing all the joys and tears, ups and downs along the way.
- My friends for bearing with my lab stories and making sure I was getting food and sleep.
- My family for allowing me to become a physics major and their attempts to read my drafts.

THANK YOU!

Table of Contents

Acknowledgements 1
Abstract 4
Chapter 1 Introduction 6
Motivation 8
Semiconductors 9
Semiconductor Physics 9
Diodes 13
Field Effect Transistors (FET) 14
Self-Assembled Monolayers 15
Why SAMs Are Great 16
How to Make an SAM FET 17
Characterization of SAMs 18
Novel System of SAMs under Investigation 19
Previous Research Findings 21
Atomic Force Microscopy 24
Conductive Probe Atomic Force Microscopy 28
Recapitulation of Chapter One 29
Chapter 2 Experimental Technique 30
Equipment 30
Preparation 30
Experimental Details 33
Control 33
Monolayer 36
More on Consistency 37
Chapter 3 Theory 38
Schottky Barrier Model 38
Tunneling Model 41
Modified Tunneling Model 46
Note on Choosing the Models 48
Chapter 4 Results and Analysis 50
Electrical Breakdown of the System 50
Current Voltage Characteristics 52

With Small Bias 53
With Large Bias 55
Resistance per Molecule 62
Hexadecane 67
Comments on Oxidation 68
Chapter 5 Conclusions and Outlook 69
Reference 71
List of Figures 75
Appendix A: 77

Abstract

Nanoscale devices are promising for the next generation of electronics, providing possibilities for greater hard drive storage capacity and higher computer execution speed. There are many strategies to produce such devices, molecular-scale electronics being a promising one. Transistors act as small switches that have a conducting channel controlled by a "gate" voltage. The gate is separated from the channel by a thin insulator. A potential design for a nanoscale transistor switch is to use a single monolayer of material that serves as both the insulator and the conducting channel.

Self-assembled monolayers (SAMs) are excellent candidates to build these tiny transistors. The novel alkyl monolayer in my study is covalently bonded to the silicon substrate, providing the insulating layer. These alkyl chains can be functionalized with a conducting molecule to provide the conducting channel. There are many technical challenges to applying voltages and measuring currents on such small devices. There lacks an encompassing model to describe semiconducting SAMs. I used atomic force microscopy to study the metal-monolayer-semiconductor (MMS) system, which is formed by bringing a conductive tip in contact with the surface. More specifically, I measured the dependence of current on the length of the alkyl chains, and compared my findings to those from existing literature on similar alkyl based SAMs. I found that the resistance of alkyl monolayers increases exponentially as the number of carbons

increases. After examining several competing models, I found that the tunneling model rather than the Schottky barrier model better describe the electron transport mechanism for the MMS system under investigation.

Chapter 1 Introduction

Self-assembled monolayers (SAMs) of organic semiconducting materials attract significant research interest as candidates for the fabrication of inexpensive nanoscale molecular electronic devices, which offer great potential for revolutionizing information technology (1). The physical size of these molecules enables dense packing, which translates into higher execution speed in computers and greater storage capability in hard drives.

The challenges in characterizing these tiny SAMs comes in part from the fact that their dimensions are on the nanoscale. Electrical measurements on such small devices such as SAMs are highly sensitive to the contact area, contact angle, contact force, etc. Previous groups studied alkyl based monolayers that are attached to metals or silicon substrate through certain atoms, and extracted a parameter, known as the decay parameter, to describe the increasing resistance as the length of the molecule increases.

In this thesis study, I am investigating a novel alkyl system, where the molecules are directly bonded to the silicon substrate through a carbon-silicon covalent bond. As the first person to attempt electrical measurement on such system, I aim to extract its decay parameter, and compare it to the decay parameter of similar alkyl monolayer systems from the existing literature.

One intriguing aspect of semiconducting SAMs is that their exact electron transport mechanisms are still under debate. Several models were proposed but no consensus has been reached. In this thesis study, I explore the existing models to determine which describes our system the best.

This thesis is driven by application values of organic semiconducting monolayers, and focuses on the fundamental electrical properties of such materials. The first chapter of the thesis describes the motivations for this research. I provide background in semiconductor physics that will help to understand the models proposed for semiconducting SAMs. I describe SAMs in general, and the unique SAMs studied in this thesis research. The second chapter explains the experimental procedures, which I developed and troubleshot, to characterize the unique SAM system with our specific equipment. The third chapter lays out the three most common theories that have been used to explain similar systems, and describes the prediction that each makes. Analysis of the experimental results is presented in the fourth chapter, along with a discussion at the conclusion and limitation of the analysis. I extracted the decay parameter, whose order of magnitude is in good agreement with existing literature. I obtained current-voltage measurements that are in agreement with other groups' observation on similar SAM systems. I found that the tunneling model describes the novel alkyl SAMs better than the Schottky barrier model. After a brief summary, I discuss the next steps for this project.

Motivation

Organic semiconducting materials possess great advantages, as they are cheap, transparent, lightweight, and flexible. They demonstrate great applications in solar cells, flexible electronics, bendable displays, and many other devices. Interest in organic field-effect transistors (organic FETs) has existed since attempts to fabricate polymer based FETs were made over twenty years ago (2) . Organic FETs attract technological interest for their potential to serve as main components in flexible yet low-cost electronic circuits. An application example of such sort is flexible displays, the prototype of which has been produced with promising market potential (3). With such technology, one can have beautiful wallpapers that change colors automatically, displays that can be rolled up and stored in a pen, or big transparent screens like one would see in a sci-fi movie. It is not surprising that much research effort is devoted to organic semiconducting materials.

There are many ways to make an organic FET. Transistors act as small switches that have a conducting channel controlled by a “gate” voltage. The gate is separated from the channel by a thin insulator. A potential design for an organic FET is to use a single monolayer of material that serves as both the insulator and the conducting channel. Organic self-assembled monolayers (SAMs) are excellent candidates to build these transistors on a nanometer scale, which inspires many studies on the electron transport mechanism in organic semiconducting SAMs. A

more detailed discussion on FETs and SAMs will be presented after some basic knowledge in semiconductor physics.

Semiconductors

Semiconductor devices form an indispensable part in peoples' daily lives. Computers, automobiles, mobile phones and many other items contain components, such as diodes and transistors, which are made of semiconductors. This section will provide some background in semiconductor physics, followed by a brief discussion on diodes and field effect transistors.

Semiconductor Physics

In an atom, the electrons surround the nucleus at certain levels of "allowed" orbit. As a consequence, an atom has discrete electron energy levels, as shown in Figure 1(a).

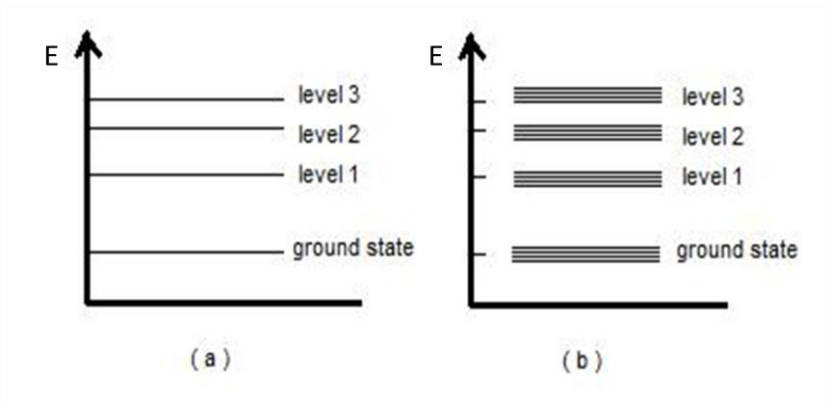

Figure 1: schematics for (a) energy levels for a single atom, and

(b) energy bands for multiple atoms

When two atoms are brought close to each other, the quantized energy levels start to split into a large number of closely spaced yet still discrete energy levels. In crystalline materials, the highly ordered crystal lattice gives distinct electron states, also called an energy band. Figure 1(b) shows the energy band structure for multiple atoms.

A "valence band" is the highest energy band occupied by at least one electron when the temperature is at absolute zero. The range of electron energies above the valence band is called the "conduction band". In semiconductors and insulators, the valence band and the conduction band are separated by a gap known as an energy gap, also referred to as the band gap, Eg, a region where electrons are forbidden to exist. The band gap of a semiconductor is smaller than 3 eV. Insulators usually have band gaps larger than 3 eV(4).

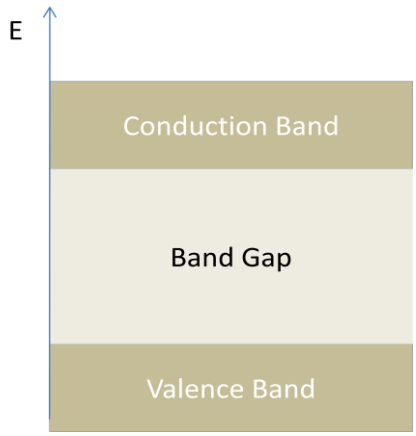

Figure 2: schematic for band gap structure

Figure 2 shows the conduction band, the valence band and the band gap schematically. In a full band, the entire range of states is occupied, and there are no available electron states to accommodate charge movement.

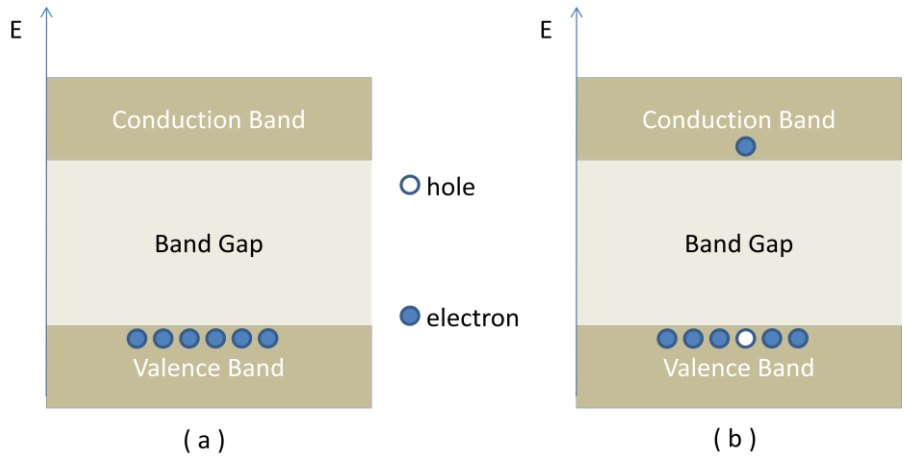

Figure 3: conduction mechanism in a semiconductor (a) the conduction band is empty whereas the valence band is full; and (b) electrons jump from the valance band to the conduction band

Figure 3 (a) shows that the valence band of a semiconductor is entirely full at absolute zero, whereas its conduction band is completely empty. This configuration leaves electrons immobilized and prevents them from conducting electrical current, thus the semiconductor behaves like an insulator. When temperature increases, electrons start to gain enough energy to jump from the valence band to the conduction band, leaving behind empty states that are known as "holes", as shown in Figure 3 (b). Both electrons and holes are free to move around to conduct electricity, and are thus called "charge carriers".

The energy band is filled from the lowest available state to the next one. When the temperature is at absolute zero, the maximum energy up to which the energy levels are filled is called the Fermi energy . The

probability that an energy level is occupied by a charge carrier can be described by the Fermi-Dirac probability density function:

<1> $$f(E) = \frac{1}{1+e^{\frac{E-E_F}{kT}}}$$

An alternative definition of the Fermi level is then the energy level whose probability of being occupied is $\frac{1}{2}$. It tells you the average energy level of charge carriers involved in carrying current. For metals, the Fermi level lies in the overlap of the conduction band and the valence band; for semiconductors and insulators, the Fermi level lies in the band gap.

In organic materials, the absence of the crystal lattice blurs the energy band edges, therefore it makes less sense to talk about the valence band or conduction band. Organic molecules form amorphous solids and it makes more sense to talk about molecular orbitals. The lowest unoccupied molecular orbital (LUMO) provides the "conduction band", whereas the highest occupied molecular orbital (HOMO) acts as the "valence band". The notion of Fermi level remains the same for organic materials, since it is a mere energy level not an energy band.

Semiconductors can be doped into n-type ("n" stands for negative) or p-type ("p" stands for positive). A semiconductor is n-type if the density of electrons in the conduction band exceeds the density of holes in the valence band, and p-type if the other way around. Both types of materials are electrically neutral because in each material, the number of protons and electrons are the same. When an n-type and a p-type semiconductors form

a junction, the electrons in the n-type semiconductor tend to flow to the other side and combine with holes, leaving behind positively charged ions in the n-type material while creating negatively charged ions in the p-type region. Theses oppositely charged ions create an electric field. It is as if the junction has a built-in potential. An external bias voltage that strengthens this built-in potential is called a reverse bias. Analogously, an external bias that weakens the built-in potential is a forward bias.

The interesting electrical property of the p-n junction makes it useful in many ways. One can use the p-n junction to make diodes for example.

Diodes

A diode blocks current in one direction and lets current flow in the opposite direction. They can be used to protect sensitive electronics from undesirable current flows. Most diodes are based on semiconductor p-n junctions discussed above. With a forward bias, only a small amount of voltage is necessary to get the current going, since the built-in potential is weakened. With a reverse bias, an ideal diode would block all current. In the real world, when the reverse bias is very large, the junction breaks down and lets the current flow. Thus a typical current-voltage characteristic of a diode, illustrated by Figure 4, often contains a region where the current is almost zero, a forward current that has an exponential dependence on the applied voltage, and a reverse current which occurs after a the junction breaks down.

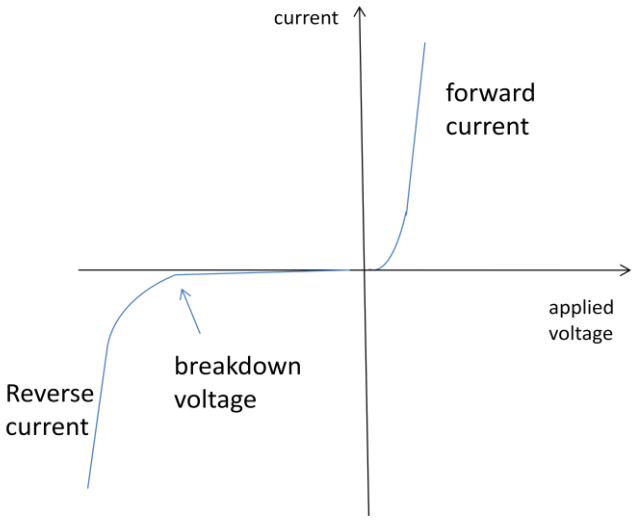

Figure 4: a typical *I-V* curve of a diode

Field Effect Transistors (FET)

As its name suggests, a FET relies on the electric field to control the current flow. A FET is either an n-channel FET or a p-channel FET, depending on the type of major charge carriers. "n-channel" means that the major charge carriers are electrons, and "p-channel" means that the major charge carriers are holes. A FET has three main components: a gate, source, and drain. Figure 5 depicts a typical n-channel FET. The region where holes are major dopant ions (indicated with "p") is often referred to as the "body".

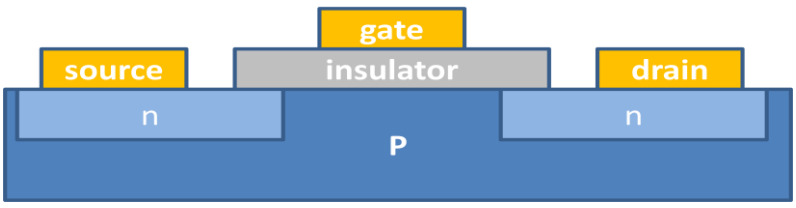

Figure 5: schematic of an n-channel field effect transistor.

In an n-channel FET, when no voltage is applied to the gate, there is no electric current between source and drain. Figure 6 illustrates what would happen when a positive voltage is applied to the gate. The electrons are attracted to the gate. Once enough electrons are attracted, a channel is built for current to flow between drain and source.

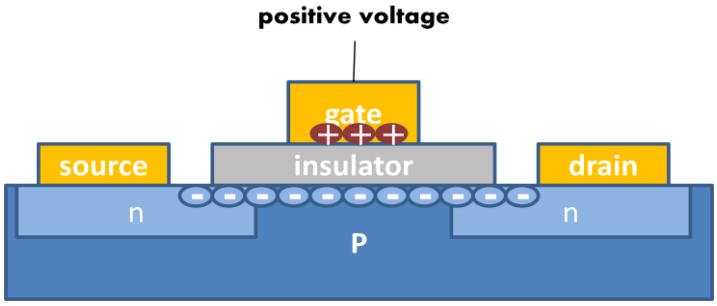

Figure 6: a schematic representation of the channel formation in an n-channel FET.

Once one knows the conducting mechanism in an n-channel FET, the conducting mechanism in p-channel FETs should be apparent. The body of a p-channel FET has electrons as its major dopant. Without a gate voltage, there is no current between source and drain. When a negative voltage is applied on the gate, the holes are attracted to the gate and build a bridge for current to flow between drain and source.

Self-Assembled Monolayers

Self-assembled monolayers (SAMs) are ordered molecular assemblies formed by the adsorption of constituents from a solution on a solid surface. As suggested by the name, the SAMs order the molecules automatically, all one needs to do is dip substrates in a liquid containing

the right molecules. Figure 7 shows the structure of an organic SAM. The headgroup of the molecules are chemisorbed (chemically bounded) to the substrate. Depending on the choice of molecules as the functional group, the monolayer can possess different properties.

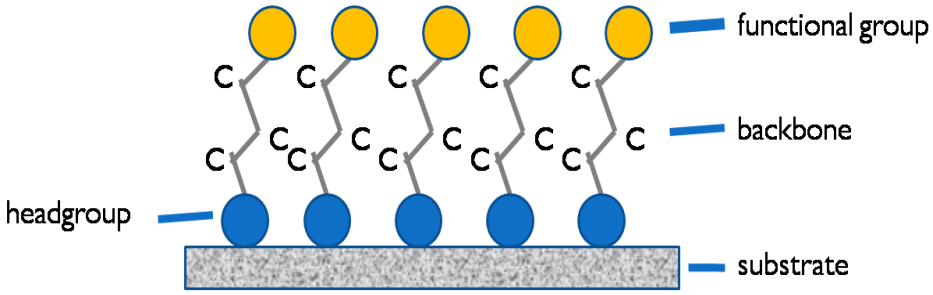

Figure 7: schematic representation of a self-assembled monolayer

Why SAMs Are Great

SAMs have attracted much research interest in the field of nanoscience, which includes studies of systems with at least one dimension being in the 1-100nm range. SAMs are nanostructures with a typical thickness of 1-3 nm, and thus an elementary form of organic thin-film material in the nanometer-scale (5). The molecules assemble themselves at the designated surface without external influences, and small quantities of molecules can cover large surface areas (6). As a natural consequence, SAMs can be prepared without ultrahigh vacuum or highly specialized equipment, and are very inexpensive to produce. In addition, SAMs are capable of providing a variety of chemically well-defined terminal functional groups to the surface, which is desirable for engineering purposes (7). In the case of a nanoscale organic FET, the monolayer providing the insulating layer can be functionalized with a

conducting molecule to provide the conducting channel, enabling current to pass through.

How to Make an SAM FET

A schematic organic FET design is shown in Figure 8. The backbone of the monolayer insulates the substrate, which takes the role of the gate in a regular FET, from the two gold pads, which act as the source and the drain. It is also worth pointing out that SAMs provide great potential to correlate macroscopic properties to microscopic ones. For example, the conductivity of the system is controllable by varying the length of molecule chains, making the whole system extremely interesting (8).

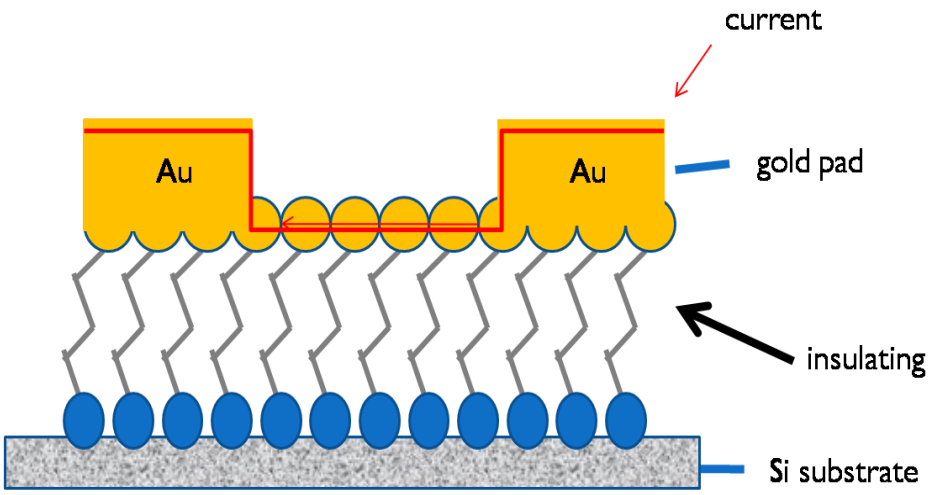

Figure 8: a schematic design for field effect transistor using organic semiconducting monolayers. The silicon substrate serves as the "gate", and the two gold pads are "source" and "drain". The backbone of the monolayer insulates the substrate, while the top of the monolayer is functionalized to conduct current.

Characterization of SAMs

Besides application values, organic self-assembled semiconducting monolayers also attract scientific interest as a tool to understand characteristics of organic semiconductors, especially the characteristic of electron transport. The spectrum of organic semiconductors widely spreads from highly ordered organic single crystals to disordered amorphous polymers, and the exact nature of electron transport in these materials is still mysterious (9). The electrons can behave as free particles or hop from one localized state to another by absorbing/emitting phonons (10). These very different electron behaviors lead to different electron transport mechanisms, from band transport to hopping transport, or the mix of the two. Knowledge of the charge carrier transport characteristic of organic semiconductors would further open vast design possibilities for organic electronics, including organic light-emitting devices (OLEDs), organic photovoltaic cell, as well as organic FETs (9). These devices have been successfully demonstrated and even used commercially. Nevertheless, a fundamental understanding is still lacking. One can achieve better designs if we understand the transport mechanisms better.

Extensive investigations have been conducted on various classes of SAMs. Initial methods are used to study their structural organization. For example, ellipsometry is used to study the sample thickness(11); X-ray photoelectron spectroscopy (XPS) is used to determine the monolayer composition(12). Recent development of scanning probe microscopies (SPM) has greatly extended the topographic understanding. SPM has also

been used as a technique to study the molecular conductivity (8) (13)(14)(15). Further discussion on scanning probe microscopy can be found under the section titled “Atomic Force Microscopy”.

Novel System of SAMs under Investigation

The electrical properties of alkyls have been studied extensively since the first observation of tunneling transport on alkane-based SAMs in 1971 by Mann and Kuhn (6) (16). This thesis focuses on unfunctionalized monolayers consisting of alkyl chains. The single bonds in the backbone of alkyl chains result in highly insulating behavior, which has been demonstrated in experiments (17)(18).

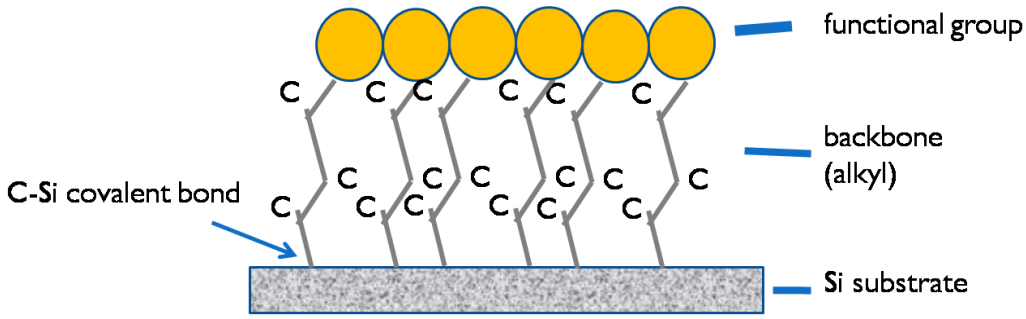

Figure 9: a schematic representation of the covalently bonded alkyls on silicon.

The novel SAM systems under investigation are produced by a facile method such that the alkyl chains are covalently bonded to the silicon substrate without the headgroup. The facile method means that the fabrication is carried out in standard glassware, at mild temperatures, and under atmosphere pressure (19). A schematic representation of the resulting SAMs is shown in Figure 9. One can modify the surface

properties of the silicon, e.g. surface potential, and potentially engineer properties of the system (20).

Three SAM samples of different molecular chain lengths are studied, which are made of alkyl with different number of carbons in the molecules: six in 1-Hexene (C_6H_{12}), eight in 1-Octene (C_8H_{16}) and 16 in 1-Hexadecene ($C_{16}H_{32}$). All of the molecules are bonded to n-type silicon substrates by free radical reactions.

In an atom, the electrons surround the nucleus at certain orbits. Free radicals, often denoted by dot ($^{\cdot}$), are atoms or molecules with a single unpaired electron. The Si-H surface can react to an arbitrary radical $R^{\cdot}$ in the following way:

$$Si\text{-}H + R^{\cdot} \rightarrow Si^{\cdot} + RH$$

$$Si^{\cdot} + R^{\cdot} \rightarrow Si\text{-}R$$

In preparation for such free radical reactions, commercially available n-type silicon was first oxidized, cleaned and rinsed with water. The oxidized silicon was then dried with an inert gas, and immersed in NH_4F to form a Si-H surface. The resulting surface is hydrophobic, with hydrogens bonded perpendicular to the surface. A H-Si bond can be dissociated under ultraviolet (UV) irradiation, or if initiated by Azobisisobutyronitrile (AIBN) with heat, as suggested by the first equation above. The broken bond makes the silicon atom a free radical, and attracts an alkane molecule. The alkene molecule breaks the double bond between

its two carbon atoms (and thus no longer an alkene), and bonds itself to the silicon atom, as the second equation above suggests. The single bond between the originally double bonded carbon atoms abstracts the neighboring surface hydrogen, leaving the neighboring silicon atom as a free radical, which attracts another alkene and the chain reaction continues. The 1-Hexene monolayer was produced using UV irradiation, while the fabrication of 1-Octene and 1-Hexadecene involves thermal assembly (initiate the free radical reactions with AIBN). All samples are provided by Isaac Moran from UMASS Amherst.

Previous Research Findings

A generic way to study the electron transport property of SAMs is to form a molecular junction of a monolayer sandwiched between the two electrodes (see Figure 10 for schematic), and study the current-voltage (*I-V*) characteristics between the two electrodes.

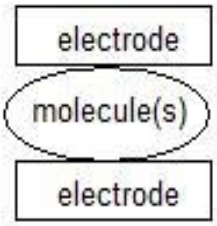

Figure 10: schematic representation of a molecular junction, with one or more molecules between the two electrodes.

The lower electrodes in this study are silicon since the SAMs under investigation are covalently bonded to silicon substrates. A wide range of

experimental results can be found on SAMs on metal substrates (21)(22)(23), and SAMs on silicon/silicon dioxide surfaces are under vigorous investigation (7) (19).

The contact between molecules and the top electrode can be chemisorbed (through chemical bonds) or physisorbed (through physical bonds), depending on the investigation methods. Mann and Kuhn used a liquid metal (mercury) to make the contact (16). Depositing a metal film on top of the organic surface by evaporation is another way to make such contact. A third way is to transfer a metal film by flotation(24). A relatively new method involves positioning a conducting probe as the electrode(6) (14) (15)(25). In this study, conductive probe atomic force microscopy (CP-AFM) is practiced as a probing method, offering control over the tip location to make physical contact with the sample.

Previous literature on alkyl systems has revealed a large energy gap (of the order of 8eV-10eV) between the HOMO and the LUMO (6) (20) (26). Consequently, these molecules are agreed to be high performance electrically insulating barriers. It is observed and expected that the tunneling current decays exponentially as the number of carbons in the molecule increases (15) (26)(27) (28). Engelkes et al used CP-AFM to study length-dependent transport in SAMs of alkanethiols and alkanedithiols with different tip-substrate combination, and found that the length decay parameter, whose meaning will be discussed in Chapter Three, to be 1.1 per carbon atom (29). The same group also found that

contact resistance of a system, which will also be discussed in the third chapter, highly depends on the electrode materials. To be more specific, platinum electrodes have the smallest contact resistance among silver, gold, and platinum electrodes (29).

A recent review article by Akkerman and de Boer summarized various research findings on alkyl-based molecules. They calculated the molecular resistance based on the results from other research groups, and found that the values for the molecular resistance from different groups share a common trend, despite the variations in the instruments used for the measurements (6).

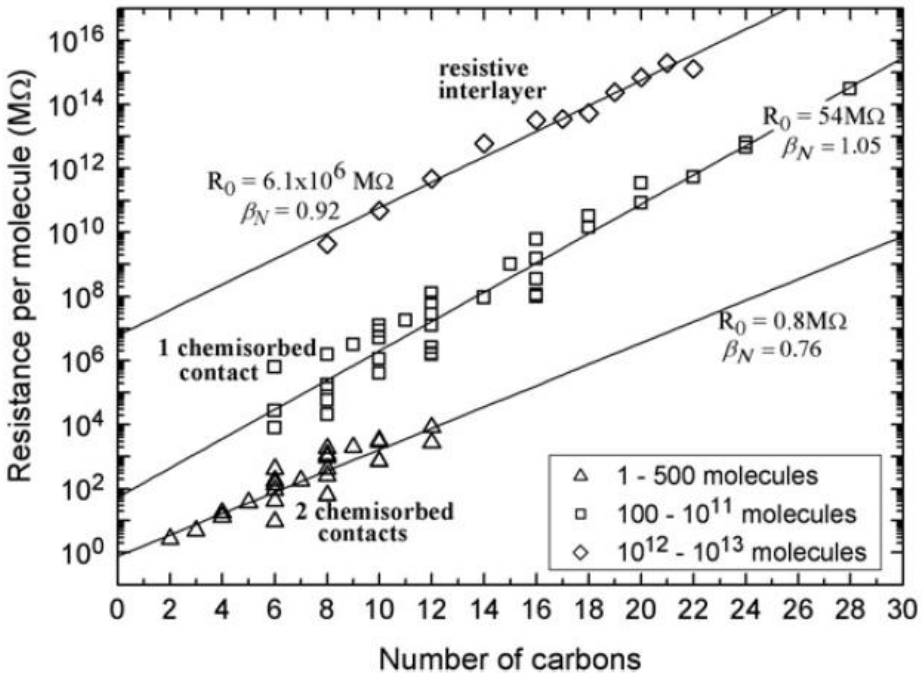

Figure 11: Akkerman and de Boer's review paper concluded exponential dependence of molecular resistance on the number of carbons in the molecule. Figure taken from Akkerman and de Boer's published work(6).

Figure 11 summarizes the trend that the values of molecular resistance can be classified into three categories, and all depend exponentially on the number of carbons in the molecules. The level of such dependence varies by the number of molecules that were contacted during measurement.

Akkerman et al. also concluded that more chemisorbed contacts lead to lower resistance, which can be tested in our experiment. One should realize that both factors, namely the number of contacted molecules and the type of contact, are very sensitive to the methods (instrument) of measurement. Further discussion on the related theories can be found in the third chapter.

Atomic Force Microscopy

Atomic force microscopy (AFM) is a type of scanning probe microscopy (SPM), whose history can be traced back to 1982, when Binnig et al. invented the scanning tunneling microscope (STM) (13). First, one will see how an STM works.

As demonstrated in Figure 12, a sharp metallic needle (the tip) is used to scan over a conducting surface at distance within the nanometer range. The tunneling current between the tip and the surface controls the tip-sample distance. The tunneling current is preselected, and an electronic controller keeps this tunneling current constant by adjusting the tip-sample distance, which is recorded as a function of the lateral position. The

limitation of STM lies in the necessity of conducting surfaces, which prevents non-conducting surface from being measured.

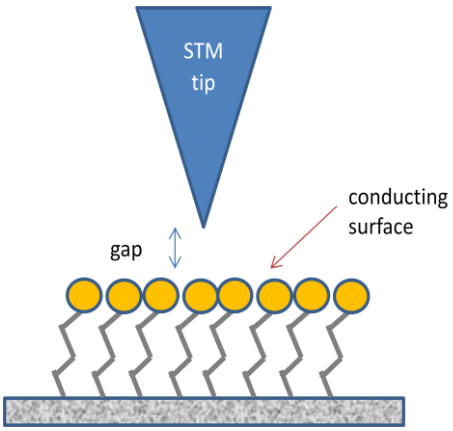

Figure 12: schematic representation of a scanning tunneling microscope.

The tunneling current between the tip and the electrode is recorded.

The invention of AFM in 1986 expanded the measurable topology to all surfaces, regardless of conductivity (30). Just like STM, AFM relies on piezoelectric materials that shrink or expand rapidly in response to change in electrical potential, as well as a feedback control.

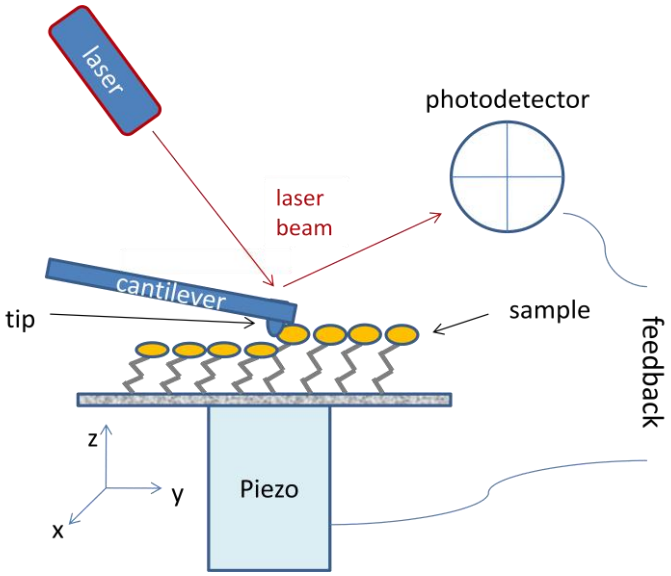

Figure 13: a schematic representation of atomic force microscopy, not to scale.

Figure 13 is a schematic representation of an AFM system. Instead of tunneling current, AFM maintains a fixed force between the probe and the surface by measuring the tip-surface force, and controlling the expansion of the z-piezoelectric materials. The x-y piezoelectric materials are used to scan across the sample. The force detection in AFM is done by shining a laser on the back of the cantilever and watching the laser spot move on the detector. A vertical fluctuation of the laser spot is captured as deflection, which is proportional to the interaction force, as governed by Hooke's law. Horizontal fluctuations are proportional to the torsional motion of the cantilever (31).

There are two common modes for topographic imaging when using AFM: contact mode and intermittent-contact mode, also known as dynamic force microscopy. In contact mode, the cantilever is scanned across a surface with a fixed deflection, with the tip in contact with the surface, as Figure 14 demonstrates. The red dotted line represents the image obtained by the AFM. This method is great for topographic information of samples with hard surfaces. Samples with soft surfaces might be damaged from dragging cantilevers across it. Intermittent-contact mode imaging is used as an alternative method. In this mode, a small piezoelectric component in the AFM tip holder drives the cantilever to oscillate around its resonant frequency. For a given cantilever, the resonant frequency, f_0, is given by $f_0 = \frac{1}{2\pi}\sqrt{\frac{k}{m_0}}$, where k is the spring constant of the cantilever, and m_0 is the effective mass that loads the cantilever. For an oscillation at

the exact resonant frequency, there is a 90º phase shift between the driving frequency and the oscillation frequency. When the tip comes close to the surface, various interaction forces between the tip and the sample, including Van der Waals force, electrostatic forces, magnetic forces, etc, modify the oscillation. The presence of these interaction forces leads to a change in resonance frequency, which results in a change of the oscillation amplitude and the phase shift. Under amplitude control, the feedback control keeps the cantilever oscillation amplitude constant. When the tip reaches a bump (or a ditch) on the sample surface, the sample stage lowers (or lifts) itself in response to a simultaneous change in amplitude. Information on oscillation amplitude, the height of the sample stage, and the phase shift is recorded as means to characterize the sample surface.

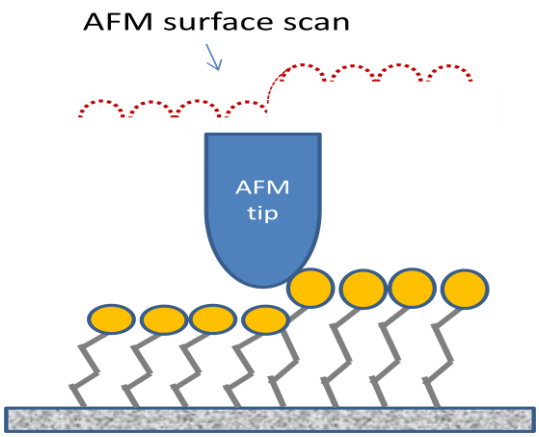

Figure 14: the AFM tip scans across the surface in contact mode, registering topological information.

Conductive Probe Atomic Force Microscopy

Although the first AFM was invented to obtain topographic images of the surface(30), it can be used to characterize additional sample properties. Conductive probe atomic force microscopy (CP-AFM), sometimes also referred to as conductive atomic force microscopy (C-AFM), is an example of using AFM to study the sample's local electrical properties. Instead of a classical AFM, a conductive tip is brought into contact with the molecules on a conducting substrate as shown in Figure 15. Electron transport through an ensemble of molecules in the SAM can be studied by applying a DC bias between the tip and the substrate.

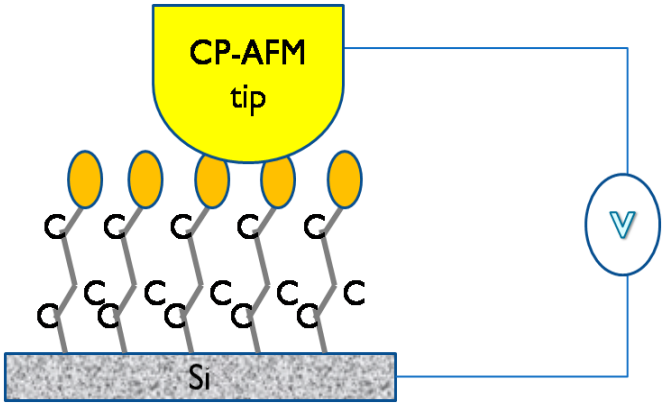

Figure 15: schematic representation of conductive probe atomic force microscopy. Bias is applied between the tip and the electrode to study the electrical properties of the sample.

CP-AFM has an advantage over STM in that the CP-AFM probe is brought in contact with the molecules, while the STM probe is kept certain distance away from the sample surface, which creates an extra tunneling gap and is likely to reduce the current.

Recapitulation of Chapter One

In this chapter, one learns the basic properties of semiconducting materials and how useful they are. One also sees that organic semiconducting SAMs are promising candidates for fabricating molecular electronic devices. A novel system of alkyl based SAMs is introduced. These SAMs should show dielectric characteristics in vertical electron transport due to the single carbon bonds in the molecule.

This thesis research uses AFM to investigate the vertical electron transport mechanisms of alkyl based SAMs of different molecular chain lengths. Details on how the experiment is done are covered in the next chapter.

Chapter 2 Experimental Technique

This chapter covers the equipment used in this thesis research, and discusses experimental setups and other details.

Equipment

The atomic force microscope and the controller are from *Asylum Research* (MFP-3D). The whole set-up is on a vibration isolation stage (TS-150 by *Table Stable Ltd*, purchased from *Herzan LLC*) in an acoustic isolation chamber (AEK 2002, from *Herzan LLC*). The software program used for the experiment as well as image analysis is Igor Pro 6.03A.

Preparation

Samples are provided by Isaac Moran from Professor Kenneth Carter's lab at University of Massachusetts, Amherst. Each sample is 1-2 cm long and 1-2 cm wide. Each sample is mounted on gold-coated slides by conductive carbon paint from *SPI Supplies Division of STRUCTURE PROBE, INC*, which offers much more reliable electrical contact than carbon adhesive tapes. A jumper wire with a magnetic end (ORCA Wire Assembly, 448.017 from *Asylum Research*) is soldered to the gold-coated slide. Each soldered junction was tested using a common multi-meter to ensure near zero (<1Ω) impedance of the junction. When not in use, the sample slide assemblies are stored in individual plastic boxes under ambient condition.

The cantilever holder is *ORCA-Dual Gain* from *Asylum Research*, which includes a built-in current-to-voltage converter. The specific holder used in this experiment is a prototype, and allows the user to choose the gain value to be either 10 nA/V, or 10 µA/V. A conductive probe is required for current measurement.

Varieties of tips have been tried, including gold-coated and platinum-coated ones. Most coated tips failed to achieve consistent current measurements. A probe made of solid Platinum from Rocky Mountain Nanotechnology (12Pt 400G No.1) with a quoted tip radius of less than 20 nm was able to produce consistent result, and has been the main probe in use.

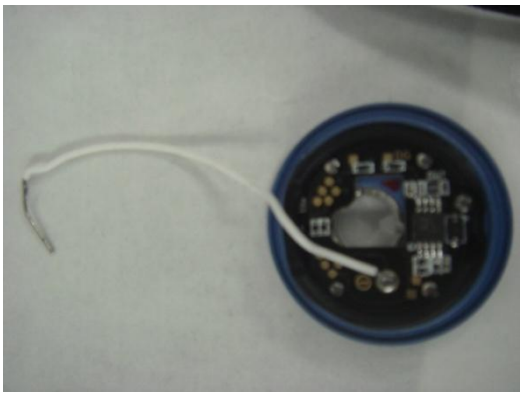

Figure 16: A photo of the ORCA cantilever holder. A jumper wire is connected to the PogoOut pin. The cantilever is mounted on the other side of the holder.

A jumper wire with a magnetic end is connected to a pin named PogoOut in the ORCA cantilever holder, a picture of which is shown in Figure 16. A jumper wire is connected to the PogoOut pin. The holder is about 3 cm in diameter. The cantilever is mounted on the other side of the holder.

The voltage on the PogoOut pin can be directly controlled by the computer. The magnetic end of the jumper wire is electrically connected to the other jumper wire (on the sample-gold slide assemble) via a small magnet, connecting the PogoOut pin and the sample-substrate assembly. When the tip is in contact with the sample surface, a closed circuit is formed.

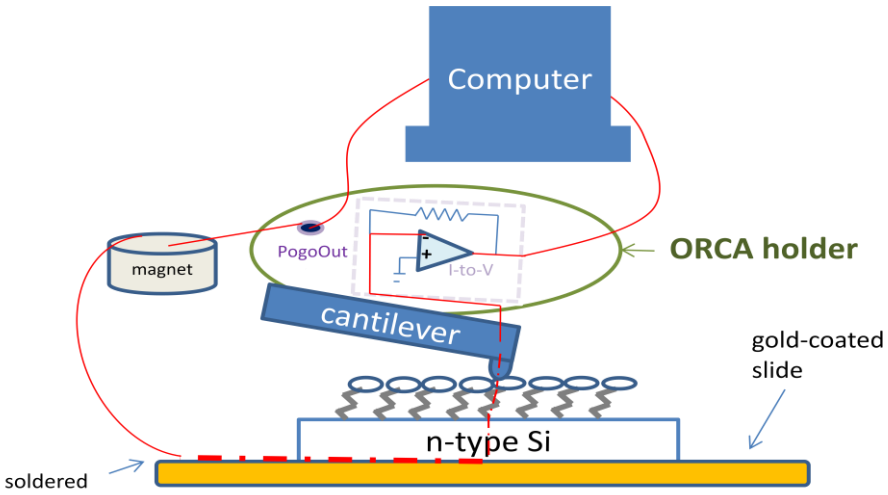

Figure 17: schematic of experimental setup, not to scale.

Figure 17 is a simple illustration of the complete setup. One can picture the red lines as wires. The closed loop is indicated by these red lines that start from the computer, connecting the PogoOut pin in the ORCA cantilever holder, reaching the slide-sample assembly via jumper wires, before passing the current-to-voltage converter in the ORCA cantilever holder that is connected back to the computer. One can use the computer to apply a bias voltage to the surface of the sample holder through PogoOut. The responding current through the tip is measured and plotted simultaneously together with the bias voltage. ORCA's maximum

voltage output is 10V, and the bias range is set by changing the voltage amplitude in Igor Pro.

Experimental Details

Control

A control experiment was carried out on a plain gold-coated slide and a 10MΩ resistor, which is connected to other components using BNC connectors. A platinum-coated tip (Electri-Lever AC240TM) was brought into contact with the surface of the slide. A non-contact mode image was obtained for selecting points for electrical measurement. After a point was randomly selected using "pick a point" in Igor Pro, the tip was moved to that point and engaged to contact the surface under examination, as shown in Figure 18.

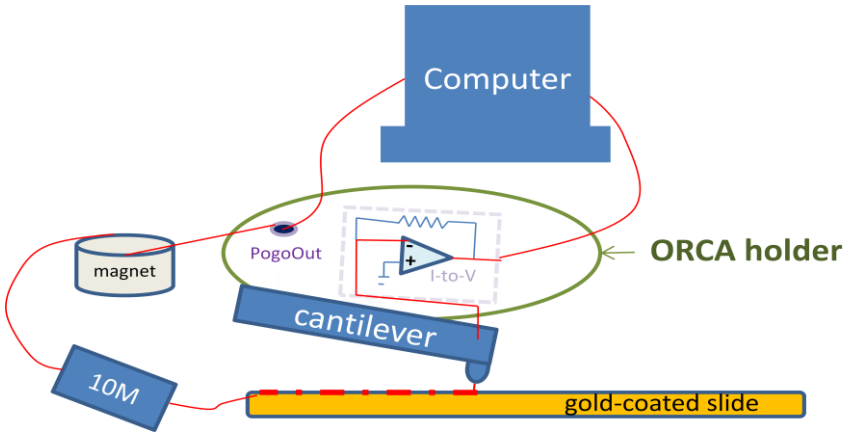

Figure 18: schema for the control setup—the sample is replaced by a gold-coated slide and a 10MΩ resistor.

Once the tip was in contact with the slide and formed a closed loop, a bias was applied to the resistor by the cantilever holder, with the bias voltage ranging from -1V to 1V.

Figure 19 shows four cycles of applied voltage of amplitude 1V as a function of time. The voltage is applied as a function of time. In this thesis research, one cycle means that the applied voltage starts at zero, increases to the desired upper limit, and starts to decrease until reaching the lower limit, and increases again to zero. Symmetric upper and lower limits are used throughout this experiment for convenience.

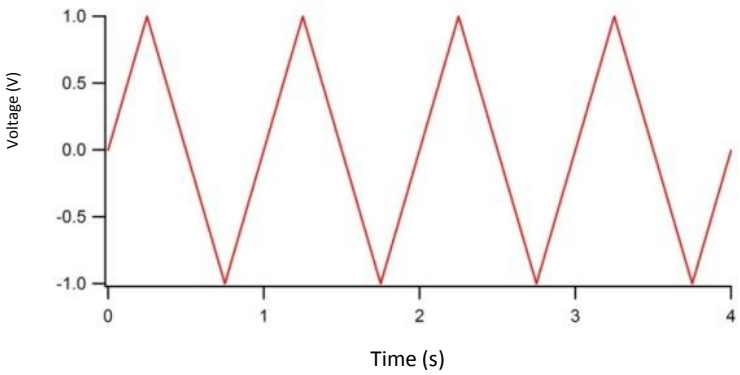

Figure 19: applied voltage as a function of time, from -1V to 1V, four cycles.

Figure 20 is a current voltage measurement (*I-V* curve) obtained by sweeping an applied voltage of amplitude 1V. Figure 21 is the averaged *I-V* curve from sweeping the bias ten times at a rate of one second per cycle.

The current-voltage plot in Figure 20 and Figure 21 can be considered identical, indicating that sweeping the voltage repeatedly and averaging will hardly affect the measurement. The obtained I-V curves are a straight line, as expected for a regular resistor. Linear fits using $y(x) =$

$a + bx$ show that the slopes of the curves are both approximately $10 \cdot 10^{-8}(A/V) \approx 10^{-7}(\Omega^{-1})$, corresponding to the impedance value 10MΩ.

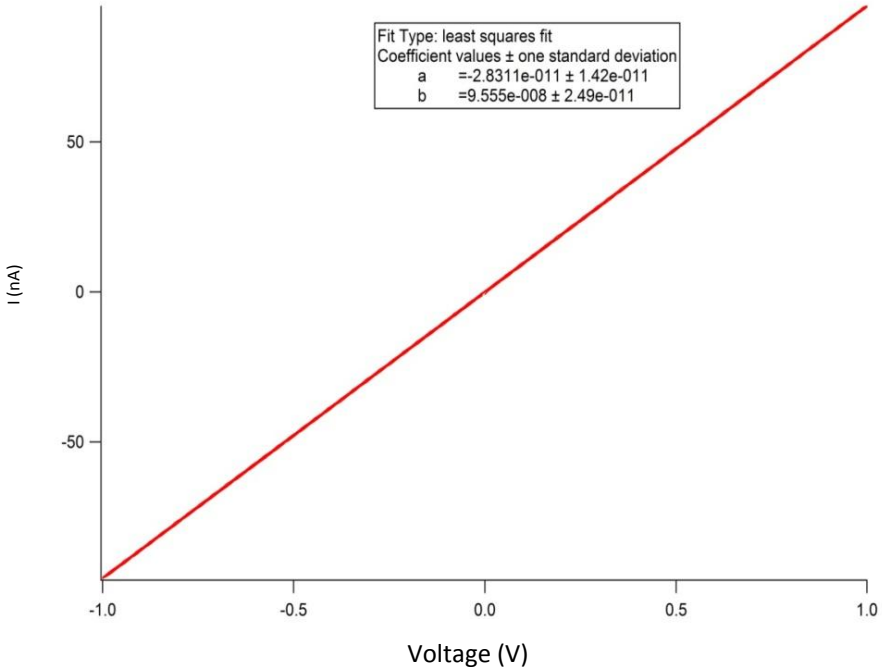

Figure 20: current-voltage measurement, voltage swept from -1V to 1V, one cycle.

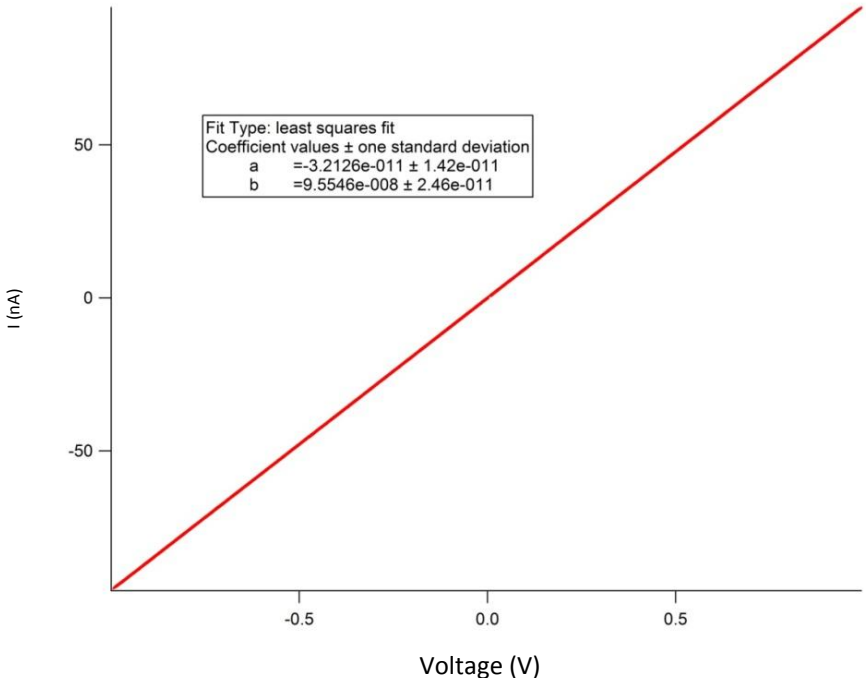

Figure 21: averaged current-voltage measurement, voltage swept from -1V to 1V, ten cycles.

The test run shows that it is possible to apply a voltage on the sample using ORCA, and that the built-in current-to-voltage converter in the cantilever holder enables ORCA to detect current correctly. The overall experiment design is plausible.

The test run also showed that that coated tips were rarely good enough for reliable current measurement. Generally speaking, only one in every four tips would work. Therefore, it is important to choose tips carefully when measuring the monolayers.

Monolayer

The measurements on 1-Hexene, 1-Octene and 1-Hexadecene based monolayers were obtained with a single probe, so there is no need to worry about the tip variation factor when comparing the results. The tip used (RMN 12Pt 400G No.1) is a solid platinum tip, and is prone to noise while imaging under intermittent-contact mode. It was possible to image in non-contact mode, but such images were often covered with noise. Since the alkyl monolayers are quite robust in general, a contact mode image was often obtained before *I-V* curves. The tip then would be moved to a point designated by the cursor, using the "pick a point" function and brought to contact with the surface. At each point, bias voltage with amplitude αV was swept, where $0 \leq \alpha \leq 10$, and the response current was measured. The frequency for sweeping the bias was kept at 1 cycle/second. The averaged I-V curves were based on four cycles. Current-voltage

curves were plotted based on two different gain values (10 nA/V, 10 µA/V) simultaneously. Two or more consecutive measurements were taken at each spot to ensure consistency. It was necessary to disengage the tip from the sample surface and reengage it from time to time, ideally before each measurement, in order to avoid electrical charge building up at the apex of the tip. It was also necessary to experiment at different points on the sample surface in order to find a good spot where one can get reliable contact and consistent measurements. (For a step-by-step instruction on how to use ORCA, please refer to Appendix A.)

More on Consistency

Prior findings by other groups include observations of big variance in resistance measurements on alkyl monolayers using CP-AFM (32). Consistency was attempted by using the same solid metal probe for all samples, avoiding variance caused by metal work function or tip geometry. Multiple measurements were made at each spot to ensure reproducibility. Failure to create a consecutive similar shaped *I-V* curve after a seemingly promising measurement would disqualify the first curve as good measurement for analysis purpose. In order to achieve consistent and reliable measurement, it is preferable to insist on the appropriate voltage range and try different spots.

Chapter 3 Theory

In order to understand the fundamental conducting mechanism of the self-assembled semiconducting alkyl monolayers, a reasonable model is needed both as a guide for exploration, and as a reference for justification.

Various groups have proposed different models for the electron transport in alkyl based monolayers. Most groups propose the tunneling model (33; 26; 29), while others have observed effects additional to tunneling, such as temperature dependence (27; 34). In this section, three potential models will be presented, followed by a short discussion on the choice of model.

Schottky Barrier Model

The Schottky barrier model is a natural choice to describe the junction formed by AFM tip and the samples under investigation, since the Schottky barrier model captures the conduction behavior of metal-molecule-semiconductor junctions, which corresponds to the platinum tip-molecule-silicon substrate junction in our experiment.

When contact is made between a metal and an n-type semiconductor, electrons tend to flow from the semiconductor conduction band into the metal. The charge on the metal-semiconductor interface changes the band structure, so that the Fermi level of the semiconductor lines up with the Fermi level of the metal, during which a potential barrier is created.

Figure 22(a) shows the band structure of a metal and a semiconductor when they are not in contact. One can contrast Figure 22(a) with Figure 22(b), where the bands form an electric potential barrier, which electrons need to overcome to flow from the semiconductor into the metal.

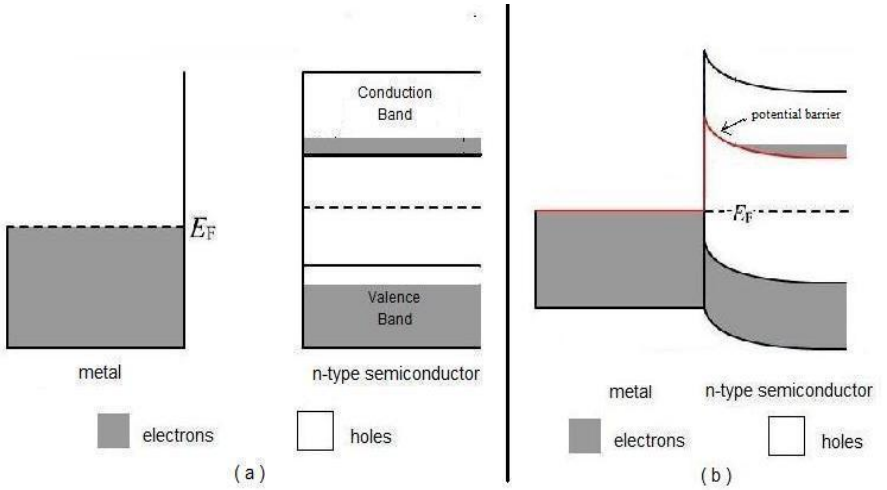

Figure 22[1]: (a) energy levels for a metal and an n-type semiconductor, not in contact; (b) Fermi levels line up when the metal and the semiconductor are in contact

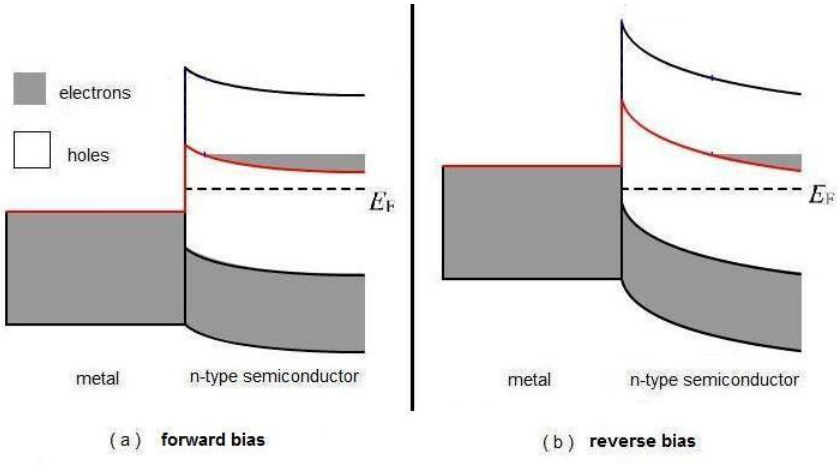

Figure 23[2]: (a) small potential barrier with forward bias, and (b) big potential barrier with reverse bias.

[1] Graphs based on a flash tutorial from: http://www.ee.byu.edu/cleanroom/semiconductor_properties.phtml

Figure 23 (a) shows a forward bias, where the potential barrier is smaller. A voltage is applied across the junction that reduces the built-in voltage of the contact. A large current flows into the metal. Figure 23(b) shows a reverse bias, where the barrier is greater. The applied voltage across the junction increases the built-in voltage of the contact. Very little current flows into the metal.

In the Schottky barrier model, the current density is:

<2> $$J = A^{*}T^{2}e^{\frac{-q\,\Phi_S}{kT}}(e^{\frac{qV}{nkT}} - 1)$$

Here A^{*} is a constant called Richardson constant ($2.52 \times 10^{6}[Am^{-2}K^{-2}]$ for n-type silicon); k is Boltzmann's constant; T is temperature; V is the applied bias; Φ_s is the Schottky barrier height; n is the ideality factor and is defined as $n = \frac{1}{1-\frac{d\Phi_S}{dV}}$. The ideality assumptions are that both materials are pure, and that there are no interaction or interfacial layers between the materials. When the Schottky junction is ideal, the barrier height is independent of the bias and the ideality factor $n = 1$. The values n is often extracted from experimental data. The current I is an integral of the current density: $I = \int_S J \cdot dA$, where A denotes contact area. It follows that the current I depends exponentially on the Schottky barrier height.

The exponential term in equation <2> can be approximated using a Taylor expansion, which in the small bias range yields:

---

[2] Graphs based on a flash tutorial from:
http://www.ee.byu.edu/cleanroom/semiconductor_properties.phtml

<3> $$J \approx A^* T^2 e^{\frac{-q\,\Phi_S}{kT}} \frac{q}{nkT} V$$

Notice that equation <3> suggest that under small bias limit the current density is linearly dependent on the applied voltage, which means that the responding current (assuming constant contact area) also depends on the bias voltage linearly.

Tunneling Model

Most research uses the tunneling model of electron transport due to the particular metal-molecule-metal junctions (27) (28)(29), but one should not rule out this model for metal-molecule-semiconductor junctions. In fact, studies on metal-molecule-semiconductor junctions have compared the Schottky barrier model with the tunneling model, and favored the latter (33). The doped silicon behaves like metal, and it is reasonable to expect tunneling behavior in the system. This section is a brief discussion on the tunneling model.

Using the knowledge from the previous section on "Semiconductor Physics", one can construct simple diagrams of the band structure in our metal-molecule-semiconductor junction. Figure 24 is an energy band diagram of a metal-molecule-semiconductor junction, without bias. The metal is platinum, as is the tip material in the experiment; the molecule is alkyl with length *l*; and the semiconductor is n-type silicon as in our case. E_c, E_v , $E_{F,}$ E_i of the semiconductor denote the energy level of the conduction band, the energy level of valence band, the Fermi energy,

intrinsic level (Fermi level without doping) respectively. Notice that the Fermi level lies in the gap between the LUMO and HOMO of the molecules, indicating tunneling is the conducting mechanism. The molecules form a potential barrier between the metal and the semiconductor.

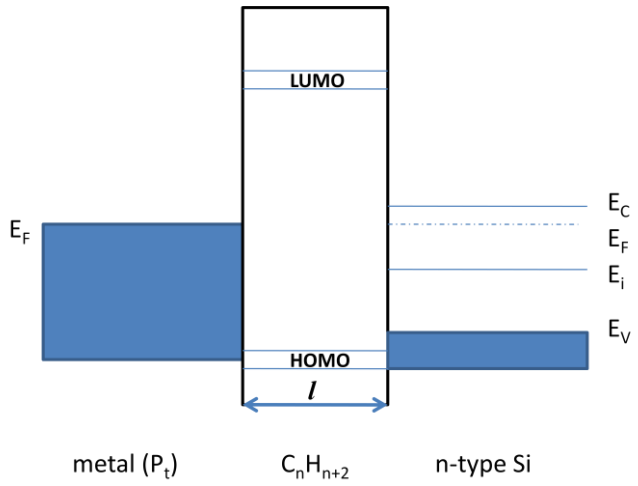

Figure 24: energy band diagram of a metal-molecule-n type semiconductor junction without applied voltage

Biasing the junction with positive or negative voltages leads to a change in the interface. Consider an n-type semiconductor (Si). Figure 25 shows the energy band of a metal (Pt)-molecule-semiconductor (n-type Si) junction when a positive voltage (V>0) is applied to the metal (Pt). The valence-band edge E_v bends downward near the interface. The conduction-band edge E_c also bends downward, getting closer to the Fermi level. The band bending causes an accumulation of electrons near the semiconductor surface.

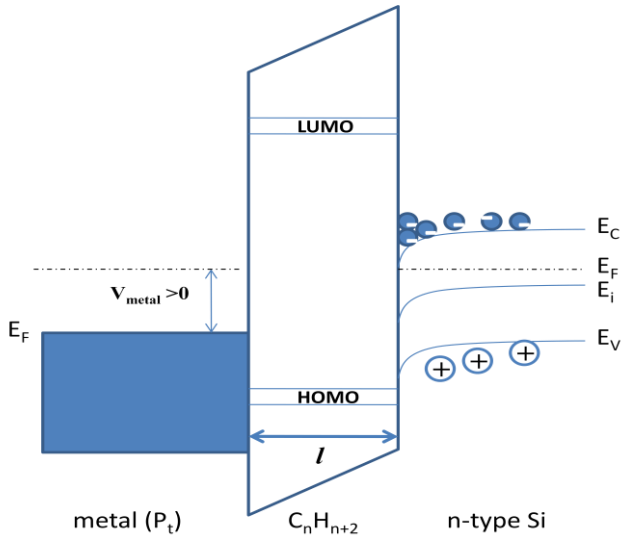

Figure 25: energy band diagram of a metal-molecule-n type semiconductor junction, with positive bias on the metal

When a small negative voltage is applied, the bands bend upward, and there are few electrons at the interface, as shown in Figure 26 (a) below. Figure 26 (b) shows that when a larger negative voltage is applied, the bands bend even more upward, and the intrinsic level crosses over the Fermi level at the interface. The number of holes at the interface is greater than the number of electrons.

Notice that no matter what voltage is used to bias the metal, the Fermi level of the metal as well as that of the semiconductor both always lie in the band gap between the LUMO and HOMO of the molecules. These diagrams are very much like the ones that depict Schottky barrier model, but with a potential wall between the metal-semiconductor interface, caused by the highly insulating molecules.

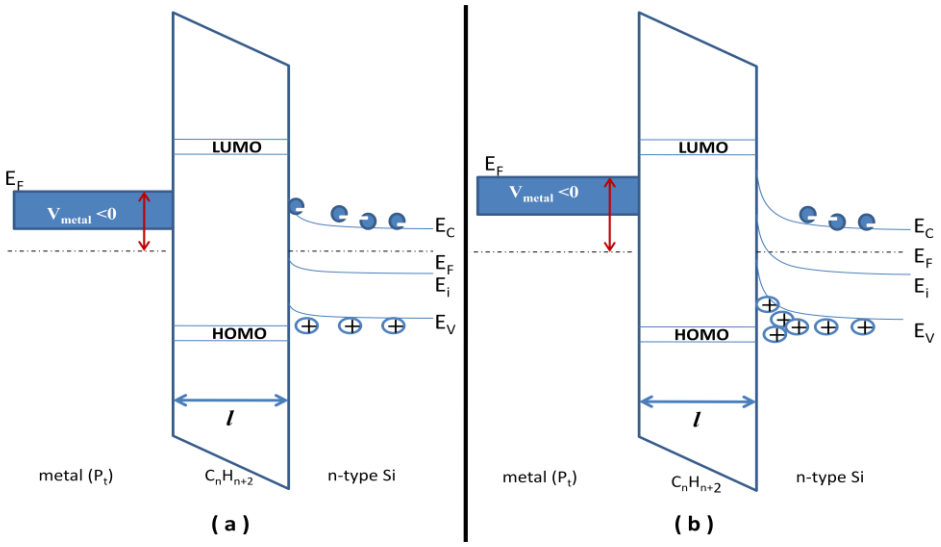

Figure 26: energy band diagram of a metal-molecule-n type semiconductor junction, with (a) small negative bias on the metal; (b) big negative bias on the metal

The Simmons model suggests that the tunneling current density can be calculated as:

<4> $$J = \frac{e}{4\pi^2\hbar l^2} \cdot \left\{ \left(\phi - \frac{eV}{2}\right) e^{-2\sqrt{\frac{2m^*\left(\phi - \frac{eV}{2}\right)}{\hbar^2}}l} - \left(\phi + \frac{eV}{2}\right) e^{-2\sqrt{\frac{2m^*\left(\phi + \frac{eV}{2}\right)}{\hbar^2}}l} \right\}$$

Here $\hbar$ is the reduced Plancks constant, meaning that $h = 2\pi\hbar$; $m^*$is the effective electron mass. V is the bias applied across the molecules (the voltage applied on the metal relative to that on the semiconductor). l is the width of the barrier, here equal to the total length of the tunneling path across molecules between the electrodes. ϕ describes the barrier height for tunneling, either through the LUMO level, where $\phi = (E_F - E_{LUMO})$, or through the HOMO level, where $\phi = (E_{HOMO} - E_F)$, and E_F is the Fermi

level of the junction as a whole. At low bias, we can rewrite expression <4> as(28):

<5> $$J \approx \frac{\sqrt{2m^*\phi}e^2}{4\pi^2\hbar^2 l} \cdot \left\{ V e^{-2\sqrt{\frac{2m^*\phi}{\hbar^2}}l} \right\}$$

from which one can conclude that the tunneling current is proportional to the applied voltage (assuming constant contacting area). In other words, a linear current-voltage curve should be expected in the low bias range. The resistance can be calculated as:

<6> $$R = \frac{4\pi^2\hbar l^2}{e^2 A\sqrt{2m^*\phi}} e^{\frac{2l\sqrt{2m^*\phi}}{\hbar}}$$

where A is the contact area. This equation can be approximated as the exponential term dominates, and is commonly replaced by

<7> $$R = R_0 e^{\beta n}$$

Here n denotes the number of repeat units (the number of carbon atoms in our case). R_0 and β can both be extracted from experiment. The interpretation for R_0 is the effective contact resistance, which can be understood as the junction resistance; and β is the tunneling decay parameter (also called attenuation factor) in units of per carbon atom. Notice that the resistance increases exponentially as the number of carbons in the molecule increases.

With high bias, the two exponential terms in expression <4> have very different magnitudes. Approximating equation <4> by the dominant exponential term yields:

<8> $$J \approx \frac{e}{4\pi^2\hbar l^2} \cdot \left(\phi - \frac{eV}{2}\right) e^{-2\sqrt{\frac{2m^*\left(\phi-\frac{eV}{2}\right)}{\hbar^2}}l}$$

which is much more complicated than in the low bias case.

Modified Tunneling Model

In general, metals and semiconductors have very different work functions, which is the minimum energy required to move an electron from the Fermi level into vacuum. This potential difference between the metal and the semiconductor is the contact potential, which should be taken into account when searching for a model. Some groups have found out that a simple tunneling model failed to account for the observed dependence of conductivity on the contact surface work function (35). One can modify the tunneling model by accounting for the effect from the electrode-molecule contact. When applying a bias across the electrode-molecule-electrode junction, the current *I* is given by:

<9> $$I = GV$$

Here *V* is the applied bias and *G* is the conductance.

The Landauer Formula, first published in 1957 and now a standard model for current computation in nanoscale devices, gives a general description of one-dimensional ballistic tunneling current (36). Ballistic means that electrons are scattered without energy dissipation. Using one-dimensional approximation is the approach most groups take before a better approximation is agreed upon. According to the Landauer Formula, the conductance *G*, is:

<10> $$G = \frac{2e^2}{h}T$$

T is a transmission function that describes the efficiency of electron transmission from one contact to another, which can be divided into three components in the modified tunneling model:

<11> $$T = T_{top} \cdot T_{mol} \cdot T_{bot}$$

T_{top} gives the efficiency of charge transport across the top contact, while T_{bot} gives the efficiency across the bottom contact, which will be discussed in the next section. T_{mol} reflects the charge transport through the molecule. A gross estimation is as if the electrons are tunneling through a rectangular barrier. In this case:

<12> $$T_{mol} = e^{-\beta l}$$

l is the width of the barrier, here equal to the total length of the tunneling path across molecules between the electrodes, and β is the tunneling decay parameter as discussed in the tunneling model. Notice that in the tunneling

model, equation <7> was written in the way that the unit of β is per carbon atom. B can also be written in a form with unit being (length)$^{-1}$, in which case $\beta = 2\sqrt{\frac{2m^*\left(\phi - \frac{eV}{2}\right)}{\hbar^2}}$. One obtains:

$$<13> \qquad I = \frac{2e^2}{h} \cdot T_{top} \cdot T_{bot} \cdot e^{-2\sqrt{\frac{2m^*\left(\phi - \frac{eV}{2}\right)}{\hbar^2}}l} V$$

when $\phi \to \frac{eV}{2}$, the tunneling current I, and the applied bias V, will show an approximately linear relationship. T_{top} and T_{bot} are not explicitly defined in the tunneling model. T_{top} corresponds to the tip-sample contact and T_{bot} describes the C-Si covalent bond. Both terms are dependent of the applied voltage. The existence of these two terms requires careful interpretation of experimental results.

Note on Choosing the Models

Many groups use the tunneling model. Degenerately doped silicon acts like a metal, so the Schottky barrier is low and electrons are likely to tunnel. To determine which model to use, one can try fitting parameters in a particular model with the experimental data. Doing so requires much fiddling around and in practice is very difficult, because this kind of measurement inherently has big variance. Before investing much time in data fitting and potentially crashing the computer memory, one can test for

the Schottky barrier model experimentally by looking at the temperature dependence.

Tunneling is a stochastic event and should be temperature independent, whereas the Schotty barrier model suggests that, when everything else is fixed:

<14> $I \propto T^2$

Should further investigation discover the tunneling model fails to explain the conduction behavior of our system, the temperature dependency is a good test of the validity of the model choice.

Chapter 4 Results and Analysis

This thesis research aims to study the electron transport mechanism across the self-assembled alkyl monolayers. Current-voltage characteristics on various samples were obtained. This section will discuss some observations.

Electrical Breakdown of the System

When the bias voltage on the sample is so high that the electric field is strong enough to rip electron off from the atoms in the molecule, the system experiences an electrical breakdown (sometimes called "breakdown" for short). The voltage at which the electrical breakdown occurs is called the breakdown voltage.

In the early stage of this thesis project, before a sense of appropriate bias was established, electrical breakdowns of 1-Hexene and 1-Octene were observed. Such breakdown manifests itself as a sudden peak on the I-V curve.

Figure 27 is an example of an electrical breakdown of the Hexane monolayer. The negative current spike suggests that breakdown occurs at around -3.5V. Figure 28 shows an electrical breakdown of Octane monolayer. The negative current spike occurred at around -8V.

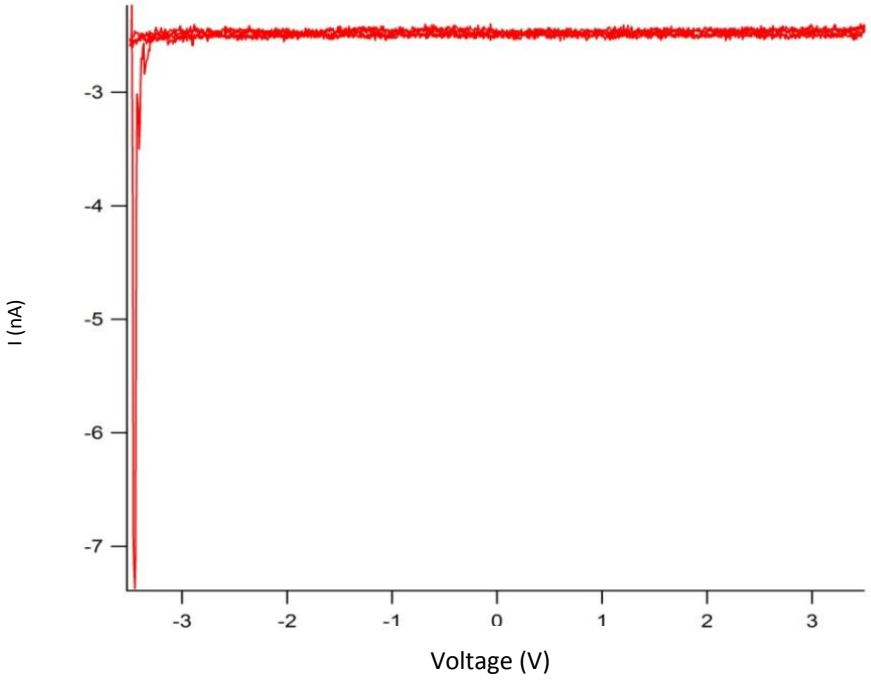

Figure 27: electrical breakdown of Hexane suggested by a negative current spike

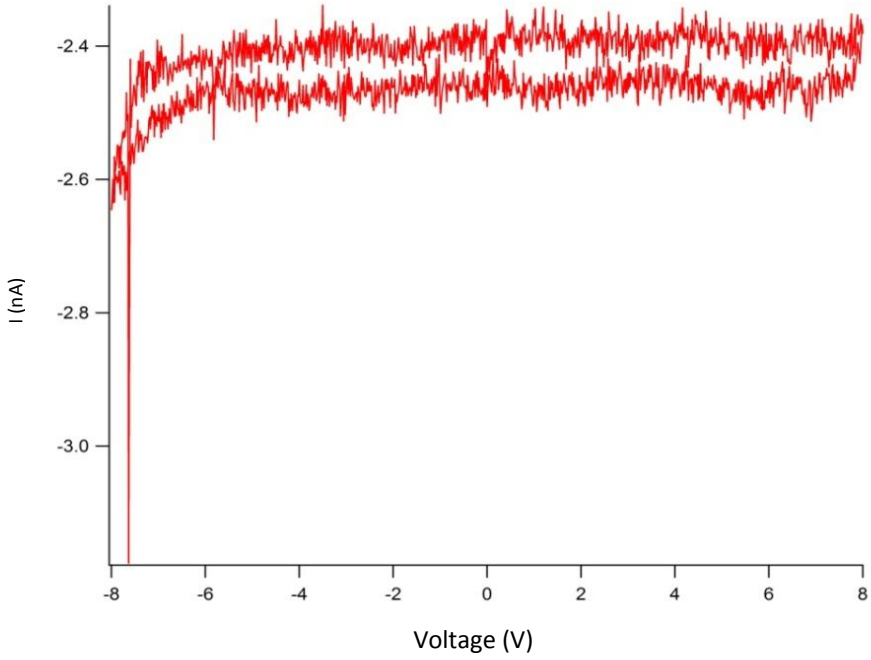

Figure 28: electrical breakdown of Octane suggested by a negative current spike

Both *I-V* curves were taken while sweeping the applied voltage at one cycle per second, 2000 points each cycle, and were unaveraged results of four cycles. The general shape of these curves was reproducible, with

small variation of the absolute number on the x-axis. Notice that the breakdown voltage of Hexane is much smaller than that of Octane, and that the resulting current of Hexane is much bigger than that of Octane. One can conclude that the Hexane monolayer is more vulnerable to electrical breakdown than Octane monolayer. The fact that the breakdown is likely to take place with negative bias is an indication that the breakdown happens as electrons move from the silicon substrate to the AFM tip.

The vulnerability of Hexane compared to Octane makes intuitive sense. Hexane molecules, each with six carbon atoms, are shorter than Octane molecules, which have eight carbons each. Everything else all equal, shorter chain length means stronger electric field, and a higher probability that electrons are ripped off.

Current Voltage Characteristics

Using the convention that bias range from -0.3V to +0.3V is “low voltage” as defined by the majority of existing literature, current-voltage characteristics can be discussed in the “small bias range” and “large bias range”.

With Small Bias

As discussed previously in the third chapter, in the small bias range, both Schottky model and tunneling model (modified or not) would expect linear current-voltage dependence.

Using the same solid platinum tip, and sweeping the bias voltage of amplitude 0.2V at one cycle per second, 2000 points per cycle, Figure 27 and Figure 28 were obtained on Hexane and Octane respectively, after averaging the data over four cycles.

Notice that, at a given voltage, more current was measured through Hexane than Octane, which is consistent with the expectation that carbon atoms reduce conductivity along the molecule.

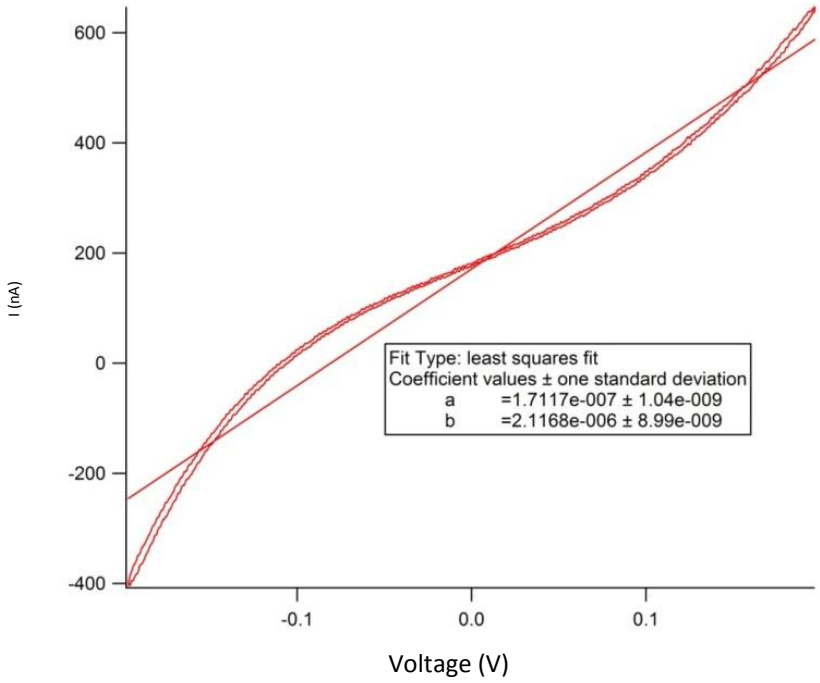

Figure 29: current-voltage measurement on Hexane, after averaging

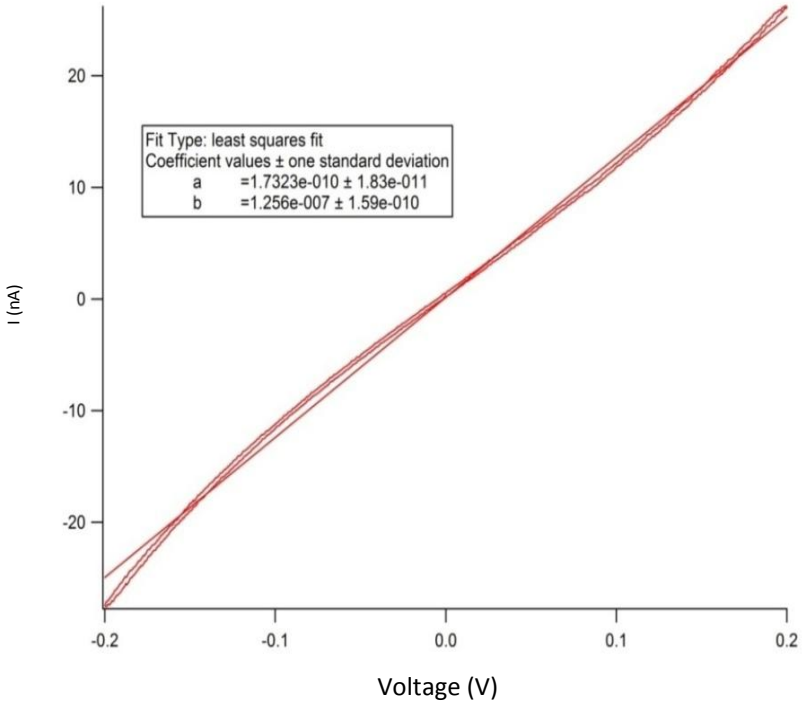

Figure 30: current-voltage measurement on Octane, after averaging

A straight line $I = a + bV$ was fitted in both Figure 29 and Figure 30, and the fitted coefficients are shown in the insets. It is evident that the resistance of the system in the low bias range can be estimated from $b^{-1} = \frac{dV}{dI}$. It follows that $R_{1C_6H_{12}} = 0.472M\Omega$ and that $R_{1C_8H_{16}} = 7.962M\Omega$. A note on the calculation is that how good the linear fit is very range sensitive. Since the linear prediction is obtained by approximating the models, one can expect the curve to be not perfectly linear. The general approach is to perform the linear fit within range smaller than the established small bias range (from -0.3V to +0.3V), and be consistent throughout the experiment. It should also be noted that the general shape of the measurement is very repeatable but the uncertainty level of the measurement is high. Depending on at what angle the tip comes into

contact with the sample, and how hard the tip is pushed (via Igor Pro software) to make the contact, the results of the measurement fluctuate wildly.

In order to reduce the effect of big measurement variance, one needs to find the averaged value for resistance measured at different points. Performing the same calculation on all the measurements with small bias to find the average values, one finds that $R_{C_6H_{12}} = 1.834M\Omega$ and $R_{C_8H_{16}} = 8.741M\Omega$. Notice that the results have changed significantly compared to the result obtained from a single spot, due to the high uncertainly level mentioned above. Using equation <7> $R = R_0 e^{\beta n}$ for n=6 and n=8, the attenuation factor (decay parameter) β is found to be 0.78 per carbon atom, which is a little higher than Engelkes' finding of 1.1 per carbon atom on Alkane(di)thiols. The contact resistance R_0 is found to be 17.02 KΩ in this thesis project, which is in good agreement with existing literature using at least one platinum electrode (29). Further discussion on the decay parameter can be found in the section titled "Resistance per Molecule".

With Large Bias

Outside of the small bias range, the current-voltage curves are expected to be sigmoid, meaning the *I-V* curves are "S" shaped. Figure 31 was current-voltage measurements on Hexane, and Figure 32 on Octane. Figure 31 was taken in the same manner as the small bias measurements, while Figure 32 was obtained from four sweeping cycles without averaging. Both voltages were swept with amplitude of at least 1V.

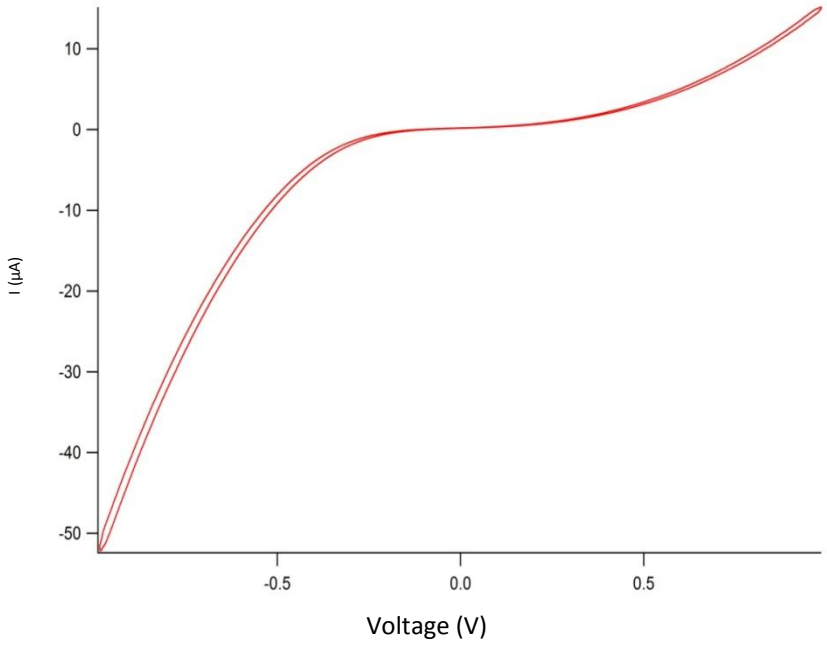

Figure 31: current-voltage measurement of Hexane

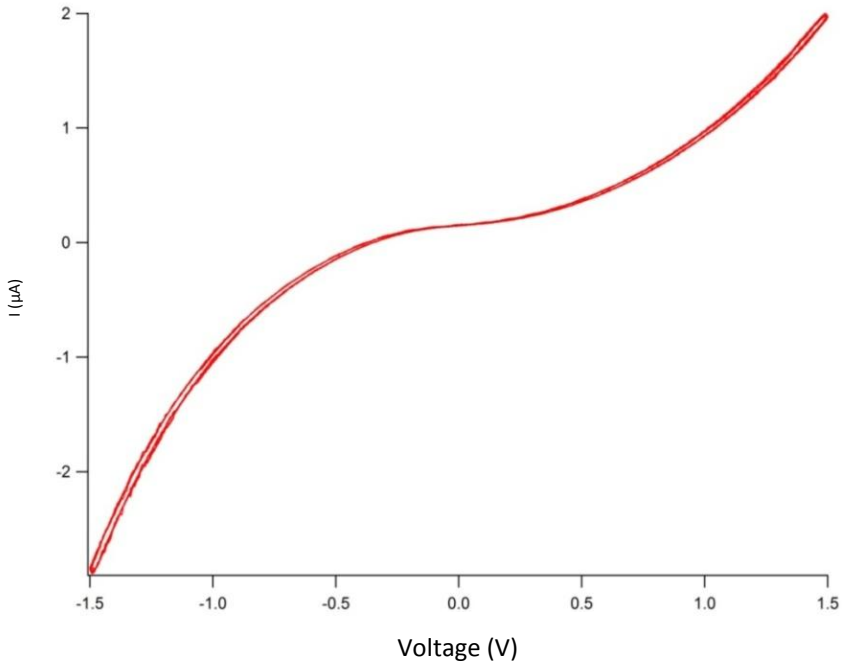

Figure 32: current-voltage measurement of Octane

Notice again, that just like in the small bias range, a larger current was measured on Hexane than on Octane for given applied voltage. For example, when the applied voltage is one volt, over 10 µA current was

measured on the Hexane monolayer, whereas only about 1μA was measured on Octane.

Asymmetric I-V behavior is observed in both Figure 31 and Figure 32 (the curves are asymmetric about zero volts). These observations suggest that the electrical behavior of the tip-molecule (top) contact is different from the molecule-substrate (bottom) contact. An alternative explanation for such asymmetry can be attributed to the electrons being the major charge carrier rather than holes, given that the silicon substrate is n-type.

There are many sigmoid functions. Specifying a model requires further data fitting. Under the Schottky barrier regime, equation <3> indicates a linear dependence of the natural log of current density on bias voltage. Since the contact area during the measurement was constant, one can conclude linear dependence of natural log of current on bias voltage. Figure 33 below is Figure 31 plotted as a semi-log plot. Judging by the naked eye, the curve is hardly linear.

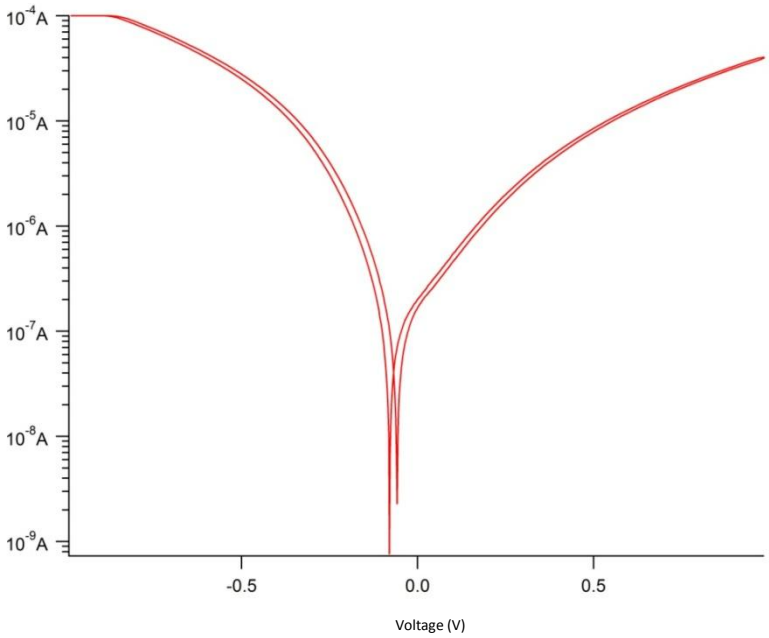

Figure 33: current-voltage measurement of Hexane, semi-log plot

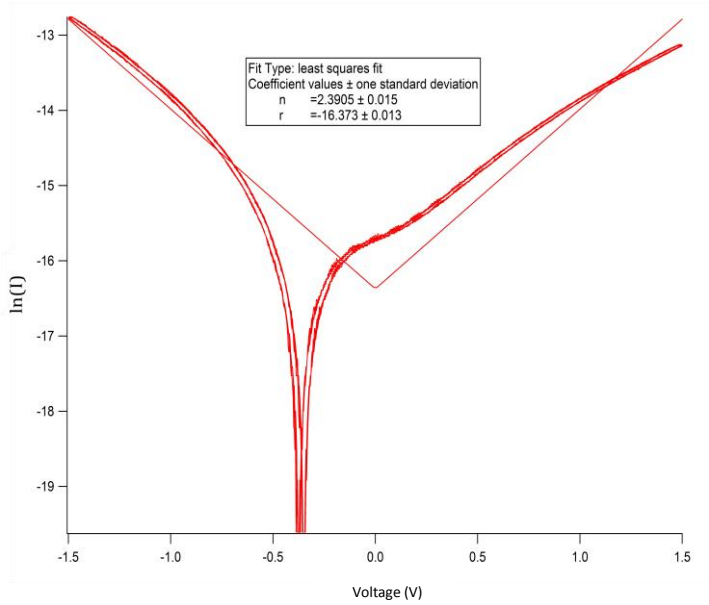

Figure 34: current-voltage measurement of Octane, asymmetric semi-log plot

Similarly, Figure 34 is a semi-log form of Figure 32. An attempt was made to fit a line described with $\ln(I) = n|V| + r$, with the fitted coefficient value shown in the inset. Notice that both Figure 33and Figure 34 are centered at a negative bias voltage, which induces high asymmetry.

This is due an offset current at zero bias caused by the built-in current-to-voltage converter.

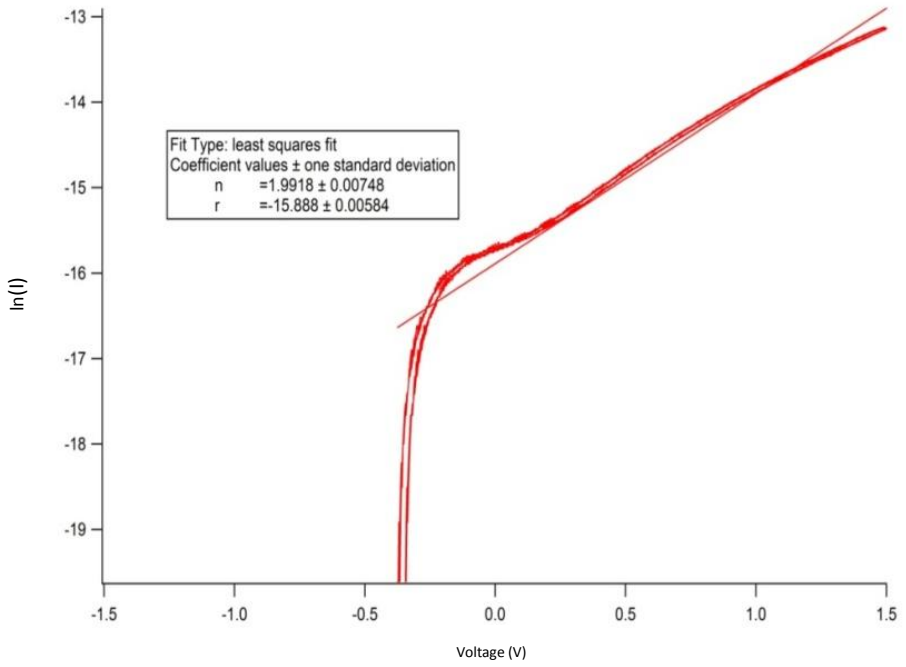

Figure 35: current-voltage measurement of Octane, semi-log plot

Removing the asymmetry substantially improved the fit, as shown in Figure 35. The fitted coefficients are shown in the inset. The standard deviation of both fitting parameter *n* and *r* decreased significantly.

According to equation <8> in the tunneling model, at high bias the exponential term dominates, and the natural log of current (density) is expected to linearly depend on the square root of bias voltage. A second attempt is therefore plotting the natural log of current against the square root of the bias voltage.

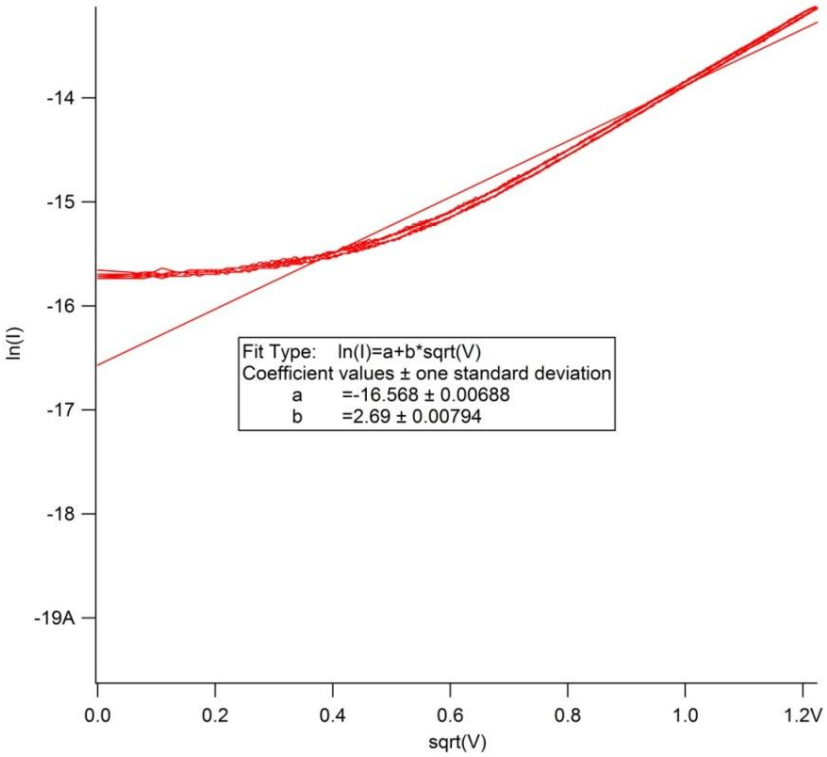

Figure 36: current-voltage measurement of Octane, transformed plot

Figure 36 is the exact same curve as Figure 32 and Figure 34, obtained on Octane. The data was transformed to make the ln(I) vs. $\sqrt{V}$ plot. A linear fit of $\ln(I) = a + b\sqrt{V}$ was performed, and the fitted coefficients are shown in the inset. Notice that compared to the fitted coefficients based on the Schottky model, the fitted coefficients based on tunneling model have comparable standard deviation.

With even larger bias, equation <3> can no longer capture the Schottky barrier model, and the ln(I) is clearly not linearly dependent on the applied voltage, as indicated by Figure 37, taken at the exact same spot as Figure 35.

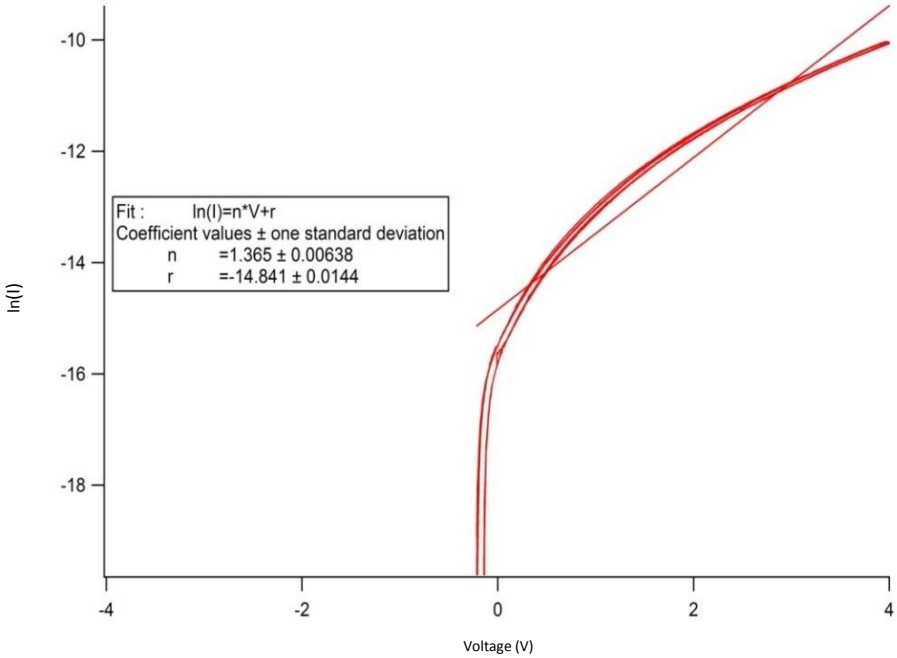

Figure 37: current-voltage measurement of Octane with large bias, semi-log plot

The fitted line in Figure 37 was $\ln(I) = r + nV$, and the fitted parameters are shown in the inset. A rough judge with naked eye would lead to the conclusion that ln(I) and V do not have a linear dependence. In comparison, the same current-voltage measurement was plotted as the natural log of current against the square root of the applied voltage in Figure 38. The blue dots indicates the fitted line of $\ln(I) = a + b\sqrt{V}$. The fitted coefficients are shown in the inset. Judging from the very small standard deviation of the fitted coefficients, the evidence that ln(I) is linearly dependent on $\sqrt{V}$ is strong. Following equation <2> in the Schottky barrier model, it is very unlikely to obtain $\ln(I) \propto \sqrt{V}$, which is suggested by the tunneling model. This is an indication that the tunneling model describes the system of interest better compared to the Schottky barrier model in the high bias regime.

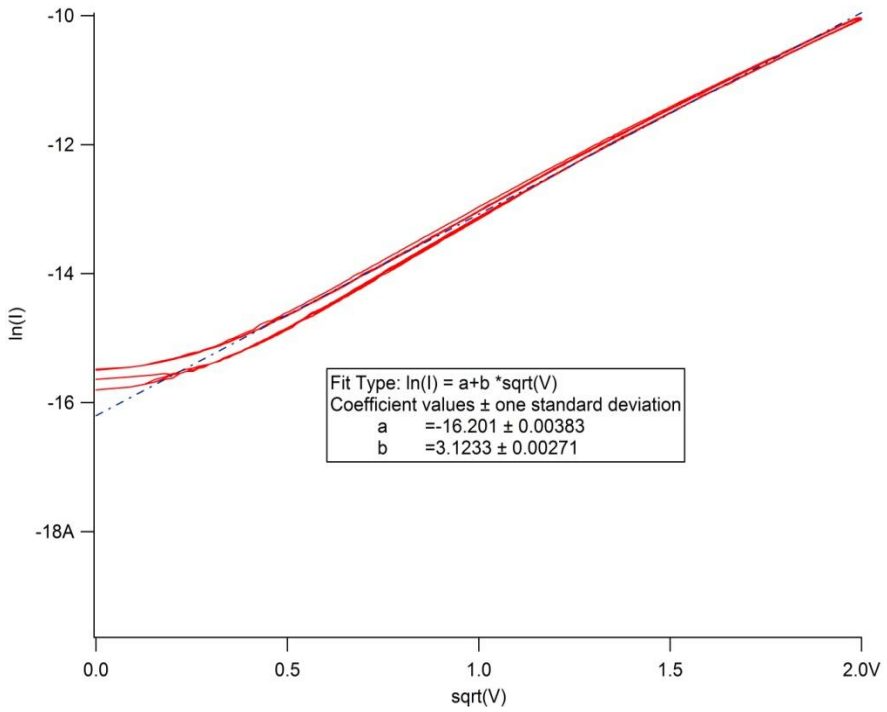

Figure 38: current-voltage measurement of Octane with large bias, transformed plot

To distinguish the tunneling model and the modified tunneling model requires better-designed experiments and careful analysis, since the two models are extremely similar. A possible approach is to change tip-substrate combination, and examine the impact of contact materials on electron transport. An easier way is to vary only tips, since varying substrates might alter molecular structure and lead to a different transport mechanism.

Resistance per Molecule

In "Previous Research Findings", we have seen a graph compiled by Akkerman and de Boer, where data on resistance per molecule based on

studies by different research groups of alkyl-based monolayers was plotted. It is surprising that the results seem to be group independent, which suggest that the experimental results from this thesis project should also be in agreement with the graph.

The value of resistance per molecule cannot be calculated without knowing how many molecules were contacted during measurement. Assuming the molecules are identical and parallel to each other, the molecular resistance can be estimated by multiplying the calculated resistance in the previous section by the number of molecules participating in the conductive process. The assumption is justified by the fact that alkyl based SAMs produced by free radical techniques contain stiff molecules that are highly perpendicular to the substrates(37).

While CP-AFM possesses many advantages as discussed in the previous sections, one disadvantage is that the contact area is quite ambiguous. We can estimate both the lower limit and the upper limit of the molecules contributing to conducting the current. If the calculation based on extreme limits are in the acceptable range, one can conclude that the real result should be at least as good as the extreme limits.

The quoted radius of the conductive AFM tip used in this thesis experiment is 20 nanometers[3]. Imaging a special sample with very small features can help to decide the tip radius. NioProbe (from Aurora NanoDevices Inc.) is such a sample with 5 nm topological features. The tip

[3] technical data sheet from Rocky Mountain Nanotechnology

radius obtained from imaging NioProbe is approximately 40 nm, greater than the quoted value. Using the 40 nm tip radius, and approximate the contact area by the formula for circular area $A = \pi r^2$, one can find the upper bound for the molecular resistance of Hexane. One should use Van der Waals radius of a carbon atom (0.16 nm) to calculate the contact area per molecule(38), since the molecules are closely packed. A brief calculation gives that each tip-sample surface contact involves approximately 62500 molecules. Recall that the tip radius used for estimation is greater than its quoted value, following which the upper bound for the molecular resistance of Hexane is about $R_{C_6H_{12}} = 62500 \times 1.834M\Omega = 114625M\Omega$, and that of Octene is about $R_{C_8H_{16}} = 62500 \times 8.741M\Omega = 546312.5M\Omega$.

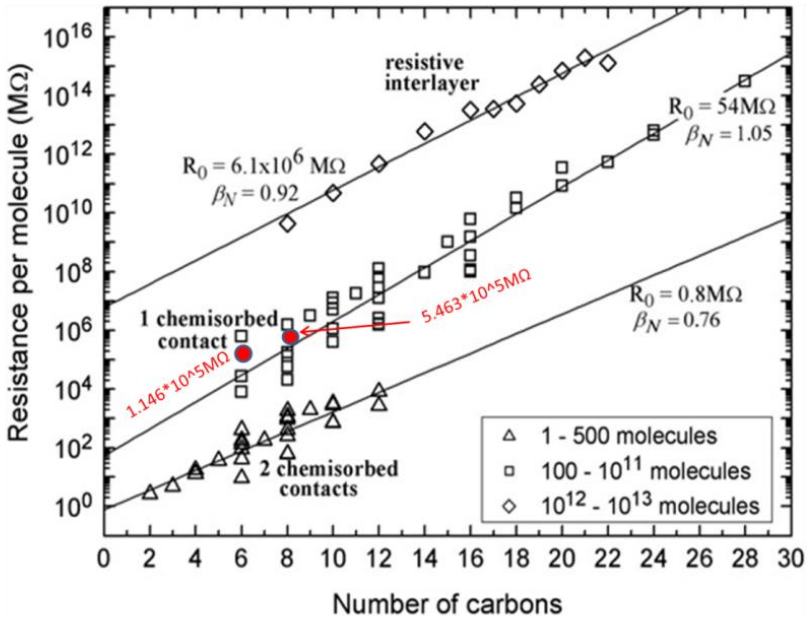

Figure 39: resistance per molecule with increasing carbon length. Red dots correspond to an intended overestimation from this thesis research.

Figure 39 shows that the upper limit of the estimated values for resistance per molecule from this thesis research, indicated by the red dots, are in good agreement with results from other research groups. The red dots are slightly above the average value from other groups, which should not be surprising, since these dots correspond to the upper limit of the results from this thesis research. Further discussion on what the two over estimated results mean can be found after the underestimated results are presented.

An alternative way to find the number of molecules in the tip-sample junction is to use existing estimates, especially the overestimated ones, since we are looking for an upper limit for our data. Akkerman et al estimated 1000 molecules were contacted during a CP-AFM experiment on alkanethiols by Beebe's group (6), who reported their metal-coated tip to be 100 nm in radius (35). This estimation seems to be an underestimate, considering the proper contact area and the atomic radius of a carbon atom. The possible explanation is that the tip geometry was taken into account. Akkerman claimed to have used the maximum grafting density of alkanethiol on gold for the estimation. A backward calculation shows that the estimated contact area was 217 nm^2. Assuming the proportionality between the contact area and the tip radius squared, a modest estimation of a 20 nm tip radius yields a contact area of 8.68 nm^2. This translates into 340 molecular contacts. The lower bound for the molecular resistance of

Hexane is then approximately $R_{C_6H_{12}} = 340 \times 1.834M\Omega = 623.56M\Omega$, and that of Octene is about $R_{C_8H_{16}} = 340 \times 8.741M\Omega = 2971.94M\Omega$.

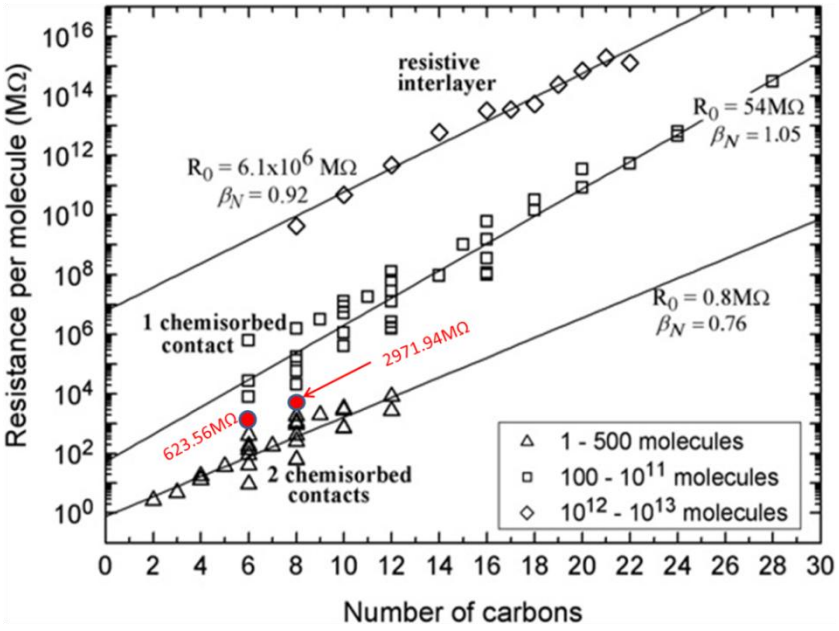

Figure 40: resistance per molecule with increasing carbon length. Red dots correspond to an intended underestimation from this thesis research.

Figure 40 shows that the lower limit of the estimated values for resistance per molecule from this thesis research, indicated by the red dots, are also in agreement with results from other research groups. The red dots are between the low resistance group (indicated by triangles) and the median resistance group (indicated by squares). The number of molecular contacts for either group seems reasonable for our setup. Notice that the measured molecular resistance for 6 carbon alkyls and 8 carbon alkyls almost form continuous lines, and our results lie in the median range.

Calculating molecular resistance does not change the decay parameter (attenuation factor) β, whose value is found to be 0.78 per

carbon atom, which is surprisingly close to the low resistance group. However, one needs to be aware that the value of β is calculated based on two points (the averaged resistance for Hexane and the averaged resistance for Octane), which is very likely to have big fluctuation with the addition of the third point. For now, one should be content that the β from this experiment has the right order of magnitude compared to other groups' results. Molecular contact resistance is highly dependent on the estimated number of molecules in contact, ranging from 1063.61 MΩ as calculated from the overestimated data, to 5.76 MΩ as calculated from the overestimated data, and should be interpreted with caution.

The upper bound and the lower bound indicate that the metal-molecule-semiconductor junctions in this thesis research are in the 1-chemisorbed contact group. This is in good agreement with our experimental setup, since our MMS junction contains a chemisorbed C-Si bond, and a physisorbed tip-molecule contact.

Hexadecane

This thesis research attempted current-voltage measurements on Hexane, Octane, and Hexadecane monolayers. Repeatable results were obtained only on Hexane and Octane monolayers. Using the calculated decay parameter β=0.78 per atom, the resistance of Hexadecane is estimated to be $R_{C_{16}H_{32}} = 11.0\ G\Omega$. The maximum bias voltage ORCA provides is 10V, giving 0.9 nA as the maximum responding current, which

is beyond ORCA's measuring ability. (Recall that the best resolution of the ORCA prototype is 10 nA.) Using a larger β will only lead to greater resistance and smaller current, which is even less likely to be detectable. In order to obtain a current greater than 10 nA, the resistance of Hexadecane should be limited to 1 GΩ, requiring β to be 0.39, which is very unlikely to be true.

Comments on Oxidation

Oxidation of an alkylsilane monolayer covalently bonded to a gold substrate was observed to affect STM current-voltage measurement by interacting with the substrate (39), and would affect CP-AFM in the same way. If the samples were affected by oxidation, their current-voltage characteristics would be identical to that of a plain oxidized silicon substrate. Attempts were made to measure the resistance of an oxidized silicon substrate, whose resistance was so strong that no current was measured, despite using multiple tips. Therefore, it is unlikely that the measurement obtained on Hexane and Octane were the effect of oxidation. Such speculation is supported by existing literature on Alkyl monolayers (37), reporting that alkyl chains with covalent bond to the silicon substrate were proved to be robust under stability tests for oxidation.

Chapter 5 Conclusions and Outlook

In summary, current-voltage characteristics of alkyl monolayers with covalent bonds to n-type silicon substrates were studied using conductive probe atomic force microscopy. An approximately linear dependence of current on applied voltage in the small bias regime was observed on Hexane and Octane, in good agreement with prior research findings on similar alkyl monolayer systems, which was predicted by the Schottky barrier theory and the tunneling theory. Current voltage plot at high bias voltage were sigmoid, and further analysis showed that tunneling theory better explains the electron transport mechanism. Calculation of molecular resistance was carried out based on experimental data. Due to the uncertainty of the number of molecules contacted during measurement, overestimation and the underestimation of molecular resistance were made intentionally. The overestimated value together with the underestimated value for molecular resistance suggested that the experimental results from this study were consistent with other groups' findings on various alkyl monolayers. Contact resistance of the alkyl systems under investigation was found to be on the small end, which can be explained by the lowered tunneling barrier due to the large work function of the platinum tip used in the study.

As predicted for alkyl systems, resistance of the system should have an exponential dependence on the number of carbons in the molecule. A decay parameter that captures such dependence was calculated to be

0.78 per carbon atom, slightly smaller than, thus has the same order of magnitude as, the average value of 0.92 ± 0.19 per carbon atom on various alkyl monolayers(6). It is expected that β will fluctuate with additional sample and corresponding data points. At this stage, one should be content that the obtained decay parameter has the same order of magnitude with the decay parameter measured by other research groups.

To verify and confirm the preliminary findings done by this thesis research, future projects can include studying current-voltage characteristics on alkyl monolayers of intermediate length, whose responding current to ORCA bias voltage should be in the detectable range. Another project can be varying the metal probe and studying the material dependence of conductive behavior of alkane systems with covalent C-Si bonds, which will also help to distinguish the tunneling model and the modified tunneling model. In addition, varing the metal probe can be used to study the effect of the metal work function in electron transport mechanisms of a metal-molecule-semiconductor junction. Ultimately, once the sample provider succeeds in functionalizing alkyl monolayers with conductive molecules, one can study the lateral electron transport mechanism by first measuring the lateral resistance between two points, and eventually map out a conductive map of the sample surface.

Reference

1. *Techonology Roadmap for Nanoelectronics.* **Compañó, Ramón.** s.l. : European Commission, 2000. Future and Emerging Technologies. Vol. II. 92-894-0170-2.

2. **Ebisawa, F., Kurokawa, T. and Nara, S.** Electrical Properties of Polyacetylene/Polysiloxane Interface. *J.Appl.Phys.* 1983, Vol. 54, pp. 3255-3249.

3. **Sirringhaus, H., et al.** High-Resolution Inkjet Printing of All-Polymer Transitor Circuits. *Science.* Dec 15, 2000, Vol. 290, p. 2123.

4. **Brown, Theodore L., Brown, Theodore E. and Murphy, Catherine.** *Chemistry: the Central Science.* 11. s.l. : Pearson Education International, 2008. 9780132358484.

5. **Love, J. Christopher, et al.** Self-Assembled Monolayers of Thiolates on Metals as a Form of Nanotechnology. *Chem. Rev.* 2005, Vol. 105(4), 1103-1170.

6. **Akkerman, Hylke B and de Boer, Bert.** Electrical Conduction through Single Molecules and Self-Assembled Monolayers. *J Phys.:Condens. Matter.* 2008, Vol. 20, 013001, p. 20.

7. **Ulman, Abraham.** Formation and Structure of Self-Assembled Monolayers. *Chem. Rev.* 1996, Vol. 96, 4, pp. 1533-1554.

8. **Krämer, Stephan, Fuierer, Ryan R. and Borman, Christopher B.** Scanning Probe Lithography Using Self-Assembled Monolayers. *Chem.Rev.* 2003, Vol. 103, pp. 4367-4418.

9. **Brütting, Wolfgang.** *Physics of Organic Semiconductors.* s.l. : Wiley-VCH, 2005. 352740550X.

10. **Mark, James E.** *Physical Properties of Polymers Handbook.* 2, illustrated. s.l. : Springer, 2006. p. 744. 0387212358.

11. **Sieval, Alexander B., et al.** An Improved Method for the Preparation of Organic Monolayers of 1-Alkenes on Hydorgen-Terminated Silicon Surfaces. *Langmuir.* 1999, Vol. 15, 23, pp. 8288-8291.

12. **Boukherroub, R., et al.** New Synthetic Routes to Alkyl Monolayers on the Si(111) Surface. *Langmuir.* 1999, Vol. 15, 11, pp. 3831-3835.

13. **Binnig, G, et al.** Surface Studies by Scanning Tunneling Microscopy. *Physical Review Letters.* 1982, Vol. 49, pp. 57-61.

14. **Cui, X. D., et al.** Bias-Induced Forces in Conducting Atomic Foce Microscopy and Contact Charging of Organic Monolayers. *Ultramicroscopy.* 2002, Vol. 92, pp. 67-76.

15. **Wold, David J. and Frisbie, C. Daniel.** Formation of Metal-Molecule-Metal Tunnel Junctions:Microcontacts to Alkanethiol Monolayers with a Conducting AFM Tip. *J.Am.Chem.Soc.* 12 2000, Vol. 122, pp. 2970-2971.

16. **Mann, Bernhard and Kuhn, Hans.** Tunneling through Fatty Acid Salt Monolayers. *J.Appl.Phys.* 1971, Vol. 42, p. 4398.

17. **Collet, J., et al.** High Anisotrpoic Conductivity in Organic Insulator/Semiconductor Monolayer Heterostructure. *Applied Physics Letters.* March 6, 2000, Vol. 76, 10.

18. **Vuillaume, D., et al.** Organic Insulating Films of Nanometer Thicknesses. *Applied Physics Letters.* Sept 9, 1996, Vol. 69, 11, p. 1646.

19. **Carter, Kenneth R.** *Oxide-Free Functional Organic Monolayers Templated by Hydride Terminated Silicon Surfaces and Their Properties.* Polymer Science and Engineering, University of Massachusetts. Amherst, MA : s.n., 2008. A White Paper Prepared for the Air Force Office of Sponsored Research.

20. **Vuillaume, Dominique.** Molecular-scale electronics. *C.R.Physique.* 2008, Vol. 9, pp. 78-94.

21. **Haiss, Wolfgang, et al.** Thermal Gating of the Single Molecule Conductance of Alkanedithiols. *Faraday Discuss.* 2006, Vol. 131, pp. 253-264.

22. **Hill, I. G., et al.** Molecular Level Alignment at Organic Semiconductor-Metal Interfaces. *Applied Physics Letters.* August 3, 1998, Vol. 75.

23. **Schreiber, Frank.** Structure and Growth of Self-Assembling Monolayers. *Progress in Surface Science.* 2000, Vol. 65, pp. 151-256.

24. **Vilan, A. and Cahen, D.** Soft Contact Deposition onto Molecularly Modified GaAs; Thin Metal Film Flotation: Principles and Electrical Effects. *Advanced Functional Materials.* 2002, Vol. 12, pp. 795-807.

25. **Moth-Poulsen, Kasper, et al.** Using Scanning Tunneling Microscopy. *Nano Lett.* 2005, Vol. 5, 4, pp. 783-785.

26. **Salomon, Adi, et al.** Comparison of Electron Transport Measurements on Organic Molecules. *Advanced Materials.* October 16, 2003, Vol. 15, 20.

27. **Cheng, Jun, et al.** Distance Dependence of the Electron-Transfer Rate Across Covalently Bonded Monolayers on Silicohn. *J.Phys.Chem B.* 2001, Vol. 105, pp. 10900-10904.

28. **Wang, Wenyong, Lee, Takhee and Reed, M. A.** Mechanism of Electron Conduction in Self-Assembled Alkanethiol Monolayer Devices. *Physical Review B.* 2003, Vol. 68, 035416.

29. **Engelkes, Vincent B., Beebe, Jeremy M. and Frisbie, C. Daniel.** Length-Dependent Transport in Molecular Junctions Based on SAMs of Alkanethiols and Alkanedithiols: Effect of Metal Work Function and Applied Bias on Tunneling Efficiency and Contact Resistance. *Journal of American Chemical Society.* 2004, Vol. 126, 43, pp. 14287-14296.

30. **Binnig, G, Quate, CF and Gerber, Ch.** Atomic Force Microscope. *Physical Review Letters.* 1986, Vol. 56, 9, pp. 930-933.

31. **Jager, Martijn de and Noort, John van.** Atomic Force Microscopy. *Encyclopedia of Life Sciences.* 2007.

32. **Engelkes, Vincent B., Beebe, Jeremy M. and Frisbie, C. Daniel.** Analysis of the Causes of Variance in Resistance Measurements on Metal-Molecule-Metal Junctions Formed by Conducting-Probe Froce Microscopy. *Journal of Physical Chemistry B.* 2005, Vol. 109, pp. 16801-16810.

33. **Wang, W., et al.** Electrical Characterization of Metal-Molecule-Silicon Junctions. *Superlattices and Microstructures.* 2003, Vol. 33, pp. 217-226.

34. **Akkerman, Hylke B., et al.** Towrads Molecular Electronics with Large-Area Molecular Junctions. *Nature.* May 4, 2006, Vol. 441, pp. 69-72.

35. **Beebe, Jeremy M., et al.** Contact Resistance in Metal-Molecule-Metal Junctions Based on Aliphatic SAMS: Effects of Surface Linker and Metal Work Function. *Journal of the American Chemical Society.* 2002, Vol. 124, pp. 11268-11269.

36. **Landauer, R.** Spatial Variation of Currents and Fields Due to Localized Scatterers in Metallic Conduction. *IBM Journal of Resaerch and Development.* 1957, Vol. 1, 3, p. 223.

37. **Linford, Matthew R. and Chidsey, Christopher E.D.** Alkyl Monolayers Covalently Bonded to Silicon Surfaces. *Journal of American Chemical Society.* Sept 10, 1993, Vol. 115, pp. 12631-12632.

38. **Tsai, C. Stan.** *Biomacromolecules: Introduction to Structure, Function and Informatics.* s.l. : Wiley-Liss, 2006. p. 4. 9780471713975.

39. **Schneider, Kevin S., et al.** The Case of the Disappearing Monolayer: Alkylsilane Monolayer Formation, Oxidation, and Subsequent Transparency to Scanning Tunneling Microscopy. *ChemPHYSchem.* 2003, Vol. 4, pp. 1111-1114.

40. **Jang, Sung-Yeon, et al.** Interpretation of Stochastic Events in Single Molecule Conductance Measurements. *Nano Letters.* 2006, Vol. 6, 10, pp. 2362-2367.

41. **Franz, W.** *Handbuck der Physik.* Berlin : Springer-Verlag, 1956. p. 155. Vol. 17.

42. **Sze, S. M. and Ng, Kwok Kwok.** *Physics of Semiconductor Devices.* 3, illustrated. s.l. : John Wiley and Sons, 2006. 0471143235.

List of Figures

Figure 1: schematics for (a) energy levels for a single atom, and..... 9
Figure 2: schematic for band gap structure..... 10
Figure 3: conduction mechanism in a semiconductor (a) the conduction band is empty whereas the valence band is full; and (b) electrons jump from the valance band to the conduction band..... 11
Figure 4: a typical *I-V* curve of a diode..... 14
Figure 5: schematic of an n-channel field effect transistor..... 14
Figure 6: a schematic representation of the channel formation in an n-channel FET..... 15
Figure 7: schematic representation of a self-assembled monolayer..... 16
Figure 8: a schematic design for field effect transistor using organic semiconducting monolayers. The silicon substrate serves as the “gate”, and the two gold pads are “source” and “drain”. The backbone of the monolayer insulates the substrate, while the top of the monolayer is functionalized to conduct current. 17
Figure 9: a schematic representation of the covalently bonded alkyls on silicon. 19
Figure 10: schematic representation of a molecular junction, ... 21
Figure 11: Akkerman and de Boer’s review paper concluded exponential dependence of molecular resistance on the number of carbons in the molecule. Figure taken from Akkerman and de Boer’s published work(6). 23
Figure 12: schematic representation of a scanning tunneling microscope..... 25
Figure 13: a schematic representation of atomic force microscopy, not to scale. 25
Figure 14: the AFM tip scans across the surface in contact mode, registering topological information..... 27
Figure 15: schematic representation of conductive probe atomic force microscopy. Bias is applied between the tip and the electrode to study the electrical properties of the sample..... 28
Figure 16: A photo of the ORCA cantilever holder. A jumper wire is connected to the PogoOut pin. The cantilever is mounted on the other side of the holder..... 31
Figure 17: schematic of experimental setup, not to scale. 32
Figure 18: schema for the control setup—the sample is replaced by a gold-coated slide and a 10MΩ resistor. 33
Figure 19: applied voltage as a function of time, from -1V to 1V, four cycles. .. 34
Figure 20: current-voltage measurement, voltage swept from -1V to 1V, one cycle. 35
Figure 21: averaged current-voltage measurement, voltage swept from -1V to 1V, ten cycles..... 35
Figure 22: (a) energy levels for a metal and an n-type semiconductor, not in contact;..... 39
Figure 23: (a) small potential barrier with forward bias, and (b) big potential barrier with reverse bias..... 39
Figure 24: energy band diagram of a metal-molecule-n type semiconductor junction without applied voltage..... 42

Figure 25: energy band diagram of a metal-molecule-n type semiconductor junction, with positive bias on the metal 43
Figure 26: energy band diagram of a metal-molecule-n type semiconductor junction, with 44
Figure 27: electrical breakdown of Hexane suggested by a negative current spike 51
Figure 28: electrical breakdown of Octane suggested by a negative current spike 51
Figure 29: current-voltage measurement on Hexane, after averaging 53
Figure 30: current-voltage measurement on Octane, after averaging 54
Figure 31: current-voltage measurement of Hexane 56
Figure 32: current-voltage measurement of Octane 56
Figure 33: current-voltage measurement of Hexane, semi-log plot 58
Figure 34: current-voltage measurement of Octane, asymmetric semi-log plot .. 58
Figure 35: current-voltage measurement of Octane, semi-log plot 59
Figure 36: current-voltage measurement of Octane, transformed plot 60
Figure 37: current-voltage measurement of Octane with large bias, semi-log plot 61
Figure 38: current-voltage measurement of Octane with large bias, transformed plot 62
Figure 39: resistance per molecule with increasing carbon length. Red dots correspond to an intended overestimation from this thesis research. 64
Figure 40: resistance per molecule with increasing carbon length. Red dots correspond to an intended underestimation from this thesis research. 66

Appendix A:
How to Use ORCA to Measure Vertical Electron Transport

A step-by-step instruction[i]:

1. Assemble the ORCA cantilever holder. Take a jumper wire from the ORCA kit, and attach the non-magnetic end to the marked[ii] small screw in the back of the cantilever holder. Leave the magnetic end hanging for the moment.
2. Prepare a conductive sample stage. If using a metal-coated slide, solder the non-magnetic end of a jumper wire onto the conductive part of the stage, and leave the magnetic end hanging for the moment. This step and Step 1 can be done in any order.
3. Mount the sample using carbon paint or silver paint so that the substrate is connected to the wire that is soldered to the sample stage. Conductive tapes are not recommended—they can be very resistive sometimes.
4. Mount the tip as usual. Remember to use a conductive probe. Bring the cantilever holder to the AFM head. Step 3 and Step 4 can be done in any order.
5. Position the sample stage on the vibration isolating stage. Put a magnet nearby so the magnetic end of the wire soldered to the sample stage has somewhere to go.
6. Turn the AFM head over as it should be done in the regular mode. Bring the hanging wire from the sample holder to the same magnet nearby. At this point, the sample stage is connected to the screw on the back of ORCA, which will be used to apply the bias voltage during experiment.
7. Proceed as usual to obtain one topographic image of the sample. Solid metal tips are harder to tune, so contact mode is often used. Coated tips should not have problems with non-contact mode imagining. One scan should be enough.
8. Position the tip by:

a. Go to the “do IV panel”;
b. Check the box in front of “show tip location”—a red dot indicating the tip position will appear;
c. Click “pick a point”, and a cursor will appear on the topographic scan that was just obtained;
d. Move the cursor to a desired spot and click “that’s it”—this will assign a number to the chosen point;
e. Click “go there” –the red dot should move to the selected point. One can hop between the old points by select the “spot number” in the drag down menu and click “go there”.

9. Make sure that “contact mode” is selected on the main panel, and engage the tip as if a contact mode scan is to be done.

10. Go back to the “do IV panel” and set the amplitude for the bias voltage, select the bias waveform from the drag down menu, enter the desired biasing rate and biasing cycle. Depending on the specific experiment, one might want to check the box in front of “average” to see the averaged result.

11. Once everything is ready, click “do it” to apply the bias voltage and measure the responding current.

12. The “force review panel” should pop up. Set the x-axis to be “bias” using the drag down menu. Select “curr” and “curr2” which correspond to currents obtained by different gains from ORCA for y-axis.

13. The default saving mode is “save to disk”. To save the plots to the hard drive, remember to check the box before “save to hard drive”.

14. If the current measurement seems to be in the wrong range, check the “nap panel” (under MFP Controls → Nap Panel) and make sure that the “ORCA sens” (sensitivity) are of correct values. If not, manually enter the correct value quoted on the ORCA kit.

15. Disengage and reengage before each current-voltage measurement for optimal results.

16. Repeat from Step 8 c) to obtain measurements on different spots.

17. To take down the set-up, simply disengage the tip, raise the head a little, remove the magnet, and take everything apart as usual.

---

[i] This guide assumes knowledge on basic (MFP-3D) AFM usage and limited experience with Igor Pro program.

[ii] In the prototype, there is a number “1” next to the screw.